Faculty of Chemistry and Chemical Engineering

Babes-Bolyai University, Cluj-Napoca

PhD Thesis Executive Summary
Synthesis and characterization of gold multifunctional nanosystems for medical applications

Superviser
Porf.Dr Mircea Diudea

PhD student:
Anamaria Ioana Orza

2011

Literature study
Introduction 3
I. Theoretical aspects of nanomaterials preparation.....7
I.1 Nucleation.....9
I.1.1 The kinetisc of nucleation 10
I.1.2 Factors that influence the nucleation.....13
I.2 Germs formation, Critical Radious.....17
I. 3 Germs growth speed.....19
I. 4 Stability of coloidal systems.....21
I.4.1 Forte de adeziune.....22
I.4.2 Electrostatic stability.....25
I.4.3 DVLO Theory 27
I.4.4 Macromolecules stability influence.....29
I.5 Adsorbtion.....30
I.5.1 Adsorbtion capacity.....32
I.5.2Factors that influence the adsorbtion.....33
II. Gold nanoparticles synthesis.....35
Introduction.....35
II.1 Metal reduction Theory.....37
II.2 Reduction in aqua media and emulsion.....39
II.3 Factors that influence the size of nanoparticles.....40
III.Coloidal systems functionalisation.....46
III.1Direct Functionalisation.....47
III.2 Ligand exchance through coupling reactions.....48
III.3 Ligand exchance through other ligands with functional groups.....49
III.3.1Factors that influence the ligand exchance.....51
III.3.2 Functionalisation of nanoparticles with biomolecules.....52
IV. Gold Nanoparticles purification 58
V. Gold nanoparticles: properties and applications.....61
V.1 Surface Plasmon Absorbtion cacacity.....62
V.1.1 Aplication based on Surface Plasmon properties.....64
V.2 Light reflexion basd on surface plasmon properties.....65
V.2.1 Aplication based on reflexion properties.....66
V.3 Catalitic properties and applications.....66
VI. Methods to characterized the coloidal systems.....68
VI.1 Spectroscopic Methods.....68
VI.1.1 IR and FTIR Spectroscopy.....68
V.I.1.2 UV-VIS Spectroscopy.....69
VI.2 Microscopic Methods.....71
VI.2.1 M TEM and SEM Microscopy.....71
VI.2.2 AFM Microscopy…….....72
Conclusions 75
Original Contributions
Introduction
I. I. Functionalization of gold nanoparticles.....78
I.1 Functionalization of gold nanoparticles with aminoacids.....83

I.1.1 Influence of pH and concentration of amino acids on the functionalization of gold nanoparticles.....83
I.1.1.1Functionalization of Glod nanoparticles with Glycine.....87
I.1.1.2 Functionalization of Glod nanoparticles with Alanine.....91
I.1.1.3 Functionalization of Glod nanoparticles with Lysine.....94
I.1.1.4 Functionalization of Glod nanoparticles with Cisteine.....97
I.1.1.5 Functionalization of Glod nanoparticles with Metionine..... 100
I.1.2 One-dimensional nanostructures based on gold nanoparticles-Amino Acids…….103
I.1.2.1 Preparation and characterization of 1D nanostructures based-lisyne/histidinaeGNP.....103
I.1.2.2 Preparation and characterization of 1D nanostructures based- aspartate GNP……..106
I.1.3 Two-dimensional nanostructures based on gold nanoparticles-aminoacids.....110
I.1.3.1 2D Nanostructure Preparation…….....111
I.1.3.2 Charactyerisation of 2D nanostructure.....112
I.1.3.2.1 *Morphological and optical characterization of 2D nanostructures*…….....112
I.1.3.2.2 *Electrical characterization of 2D nanostructures* …….....116
Conclusions…….....118
I.2 Functionalization of gold nanoparticles with proteins …….....121
I.2.1 Functionalization of gold nanoparticles with steric proteins (BSA,HSA)…….....123
I.2.1.1 Influence of BSA concentration and electrolite on the GNP functionalisation ……...124
I.2.1.2 pH influence on GNP-HSA functionalisation…….....131
I.2.2 Functionalization of gold nanoparticles with collagen ……...135
I.2.2.1 Influence of pH and reducing agents on collagen functionalization.....136
I.2.2.2 Physical-chemical characterization of functionalized collagen fibers.....141
I.2.3 Applications of collagen functionalized gold nanoparticles ……....146

Conclusions.....167
I.3 Gold nanoparticles functionalization through ligand exchange……172
I.3.1 Functionalization of gold nanoparticles with PEG-OH……172
I.3.1.1. Gold Nanoparticles preparation……...…172
I.3.1.2. Ligand exchance…….....174
I.3.2. Functionalization of gold nanoparticles with cu PEG-COOH……177
I.3.3 Functionalization of gold nanoparticles with phosphines.....178
Conclusions.....180
I.4 Functionalization of gold nanoparticles with drugs…….....181
I.4.1 Functionalization of gold nanoparticles with temozolomide …….182
I.4.2. . Functionalization of gold nanoparticles with cisplatin, doxorubicin and capecitabine ……..…....191
I.4.3 Applications of functionalized gold nanoparticles –cisplatin/ capecitabine /doxorubicin in the treatment of liver cancer.....199
I.4.4 Applications of functionalized gold nanoparticles-Temodal in glioblastoma multiform cancer …….....212
Conclusions.....219
II. Controlled destruction of subcellular structures in cancer therapy …….....221
II.1 Distrugerea controlată a structurilor subcelulare cu nanoparticule de aur activate cu laser……..223
II.1.1 Influence of gold nanoparticle concentration and laser power.....230
II.1.2 Influence of laser exposure time……..234
Clonclusions……242
Bibliography……245
Annexes……...273
Publications ……299

Introduction

One of the areas that have revolutionized the scientific and technical development is nanotechnology. Nano-scale materials have completely different properties than the macro scale ones. The secret of obtaining such nono-materials is to control their nanoclusters assemble such as to provide materials with new electronic, structural and chemical properties.Nanomaterials (particles with diameter between 1-100 nm) can be formed from any substance including metals[1-2], semiconductors [3-4], metal oxides, organic polymers. [5-9] The development of nanomaterials have revolutionized the biomedical science offering new ways of treatment and diagnosis of various diseases. Another area in which nanomaterials have potential applications is the field of electronics and electrical engineering. In this sense, carbon nanotubes due to their special properties (high thermal conductivity and high electrical, mechanical and chemical resistance) led to the development of new applications: electric lines [10], high electrical conductiv plastics [11] and electrodes for fuel electric cell 12.. From the data published by the NIST13 Institute 60% of the carbon-based nanomaterials are used as catalysts in the chemical industry.

Gold colloids are one of the oldest scientific topics studied. Gold has been used since antiquity in aesthetic and curative purposes. In the 17th century gold has been used to color glass and ceramics[22]. In 1600 Paracelsus has first published the synthesis of gold colloid ''aurum potable, oleum auri; quinta essentia auri " by condensation of auric chloride (AuCl3) in an alcoholic plant extract 23 and is considered the first synthetic drug.The first medical applications of gold colloids is in syphilis diagnosis but without significant results. Moreover, its curative effects were contested, claiming that auric tincture is devoid of any medical or therapeutic value. The development of nanomaterials has opened new ways in biomedical research (fundamental / applied) such as measuring low concentrations of bacteria, the discovery of new drug vectors 18, in the detection of certain proteins19, in separation and purification of cells and molecules 20. Also, gold

nanoparticles are widely used in the manufacture of biosensors with high specificity.

The main topic of the thesis describes the preparation of colloidal gold systems and their functionalization with different molecules for biomedical purposes.

In the theoretical part are summarized the main aspects of nucleation, growth, stability and purifications. The Personal contributions contain elements related to GNP functionalization with amino acids, proteins and drugs. Functionalization was demonstrated by specific analysis such as: TEM, AFM, FTIR, XPS, UV-VIS. The prepared aminoacids based-nanostructures were used as vectors to treat liver cancer and glioblastoma multiform tumor. The protein based-nanostructure were used to prepare nanosubstrate that sustain cell differentiation into neuronal and cardiac lines. The results obtained offer a new chemotherapy strategy for patients diagnosed with unresectable recurrent malignant gliomas and hepatocarcenoma and advanced cellular differentiation processes.

The thesis has been structured in VI theoretical chapters and II continanad original contributions. The scientific results are presented in **270** pages of the thesis such as **80** figures,**12** tables, and **239** bibliographical references of which **2** bibliographic references are personal. Note that in the summary both chapters numbers and bibliographic reference are maintained such as are presented in the thesis.

ORIGINAL CONTRIBUTIONS

I. Functionalization of gold nanoparticles

The thesis aim is the preparation of colloidal systems based on gold functionalization with different biological active molecules (amino acids, proteins, drugs) that lead to nanostructures with application in biomedical field. The target of this chapter was to obtain high property nanostructures in order to improve the quality of the drug transport for a more efficient cancer treatment. Another aim was to prepare nanoscaffolds for biosensing and for cell differentiation.

I.1 Functionalization of gold nanoparticles with aminoacids

In this chapter I studied the functionalization of gold nanoparticles with amino acid and and how the main factors (pH, concentration) influence the bond strength of the amonoacid-nanoparticule.

I.1.1 Influence of pH and concentration of amino acids on the functionalization of gold nanoparticles

From the essential and nonessential amino acids, in this thesis I choose for the study the following aminoacids: glycine, alanine, cysteine, methionine and lysine. This choice was made based on the number of NH2,-SH groups- and on the length of the hydrocarbon chain.

The changes that has occured on the coupling amino-GNP were followed experimental by UV-VIS spectroscopy using a JASCO V-570 spectrometer. Absorbance was measured at different pH values and at different aminoacid concentrations.

Characterization of gold nanoparticles

Particle size was evaluated using transmission electron microscopy (TEM), and showed an average diameter of 32 nm. (**Fig. 2)**

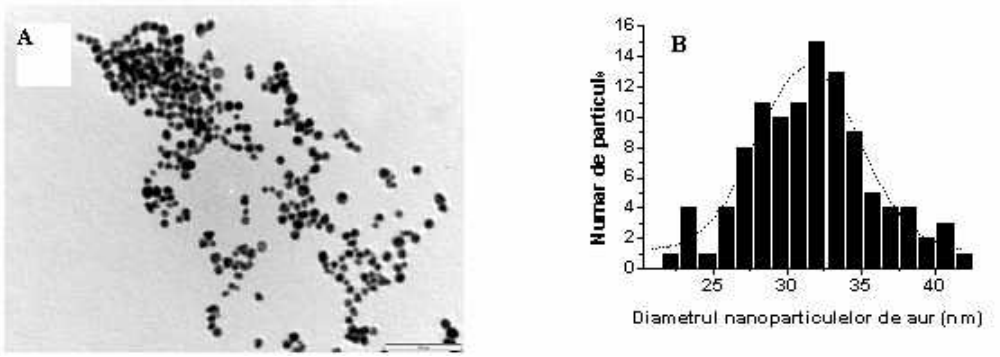

Fig.2. TEM image of gold nanoparticles of 32 nm (A) together with their distribution histogram (B) 200 nm scale (over 100 nanoparticles were analyzed)

The results of the influence of concentration and pH on the aminoacids nanostructures are presented in ***Tables 1-5***

Tab.1-Absorbance values Gly / GNP for different pH values at various concentrations concentration

pH-2		pH-4		pH-6		pH-8	
Abs (u.a)	C x10 $^{-4}$ (M)	Abs (u.a)	C x10 $^{-4}$ (M)	Abs (u.a)	C x10 $^{-4}$ (M)	Abs (u.a)	C x10 $^{-4}$ (M)
0,29	0,2,	0,336	0,6	0,32	0,3	0,644	0,3
0,238	0.7	0,317	2,6	0,3	1,3	0,601	1,2
0,173	1,7	0,28	7,6	0,262	3,3	0,516	2,1
0,133	2,7	0,242	12,6	0,229	5,3	0,44	3
		0,2	22,6	0,195	8,3	0,375	3,9
				0,168	12	0,330	4,8
				0,148	15,3	0,296	5,7
						0,270	6,6
						0,248	7,5
						0,226	8,4
						0,214	36,3
						0,185	50

Tab.2: Absorbance values Ala / GNP for different pH values and concentration

pH-2		pH-4	
Abs (u.a)	C x10 $^{-4}$ (M)	Abs (u.a)	C x10 $^{-4}$ (M)
0,206	2,0	0,271	2,0
0,185	3,0	0,242	3,0
0,234	1,0	0,303	1,0
0,166	4,0	0,217	4,0
0,151	5,0	0,194	5,0
0,138	6,0	0,171	7,0
0,128	7,0	0,152	9,0
0,115	8,0	0,134	11

Tab.3- Absorbance values Lys / GNPat different concentration and pH=2

pH-2		
Abs (u.a)		C x10 $^{-4}$ (M)
λ_1=532 nm	λ_1=640 nm	
0,179	0,17	3,0
0,153	0,161	6,0
0,138	0,152	9,0
0,127	0,139	19,0
0,114	0,124	39,0
0,100	0,105	69,0
0,086	0,092	119

Tab.4 - Absorbance values Cis / GNP for different pH values and concentration

pH-2		pH-4 8		pH-6			pH-8	
Abs (u.a)	C x10 $^{-4}$ (M)	Abs (u.a)	C x10 $^{-4}$ (M)	Abs (u.a)		C x10 $^{-4}$ (M)	Abs (u.a)	C x10 $^{-4}$ (M)
				λ_1=532	λ_2			
0,256	1,0	0,246	1,0	0,241		1,0	0,224	1,0
0,205	2,0	0,227	2,0	0,212		2,0	0,190	2,0
0,188	4,0	0,209	3,0	0,195		2,6	0,163	3,0
0,166	5,0	0,183	5,0	0,185		3,2	0,138	4,0
0,139	10	0,155	8,0	0,172		2,8		
		0,131	12	0,151		4,8		
		0,105	17	0,139		5,8		
		0,079	27					

Tab.5 - Absorbance values Lys / GNP at different concentrations and pH=2

pH-2		
Abs (u.a)		C x10 $^{-4}$ (M)
λ_1=532 nm	λ_1=640 nm	
0,144	0,145	1,0
0,122	0,134	2,0
0,109	0,123	3,0
0,095	0,107	5,0
0,075	0,087	10

The bond strength and the ligand-binding mode is strongly influenced by the pH. At a high concentration OH ions, pH = 2 the amino acid is in its cationic form. The NH3

+ group is an attractive center for GNP negative charge carrier. At intermediate pH (above the isoelectric point) the amino acid is in its anionic form. Between the negatively charged gold nanoparticulate and the negative charge of amino acid the repulsive forces appear, the coupling between the nanoparticule and the amino acid occurs through weak Van der Waals force.

It appears that increased levels of amino acid amino acid increases its adsorbtion on the surface of nanoparticles . By representing the adsorbtion as a function of pH (Abs / pH) for different concentrations of amino acid there is a change in slope near the isoelectric point, absorption beeing maximum at this point.

As lysine concentration increases, the absorbance decreases, with the peak deformation, so that at the concentration lys = 9 x10-4 M are two wavelengths appears λ1 = 532 nm respectively. λ2 = 640 nm The appearance of the second maximum is determined by the agglomeration of nanoparticles in nanowires.

I.1.2 One-dimensional nanostructures based on gold nanoparticles-Amino Acids

In recent years, gold nanoparticles have been intensively studied due to their interesting optical properties with potential applications in biomedicine. Gold nanoparticles can self-assembly into highly anisotropic nanostructures by using biomolecules either as capping agent or as a template (amino acids, DNA, collagen) [190 -193]

Amino acids are a class of biomolecules which were successfully used to cap metallic nanoparticles of silver and gold They can have various binding sites like *thiol* group, *α*- and the *side-chain amine* groups and *α-carboxylic* group[194-198]

Experimental

L-Lysine-capped gold nanoparticles (Lys-AuNPs) Lysine-capped gold nanoparticles were prepared as following described: 1ml L-lysine (0.075% in water) was added in 100 ml of $HAuCl_4$ (0.01%); after stirring the solution for about 5 minutes, 1 ml of reducing agent was put into the solution (0.075% $NaBH_4$). The solution was vigorously mixed again for another 5 minutes, centrifuged at 15000 rpm for 15 minute and washed with double distilled water.

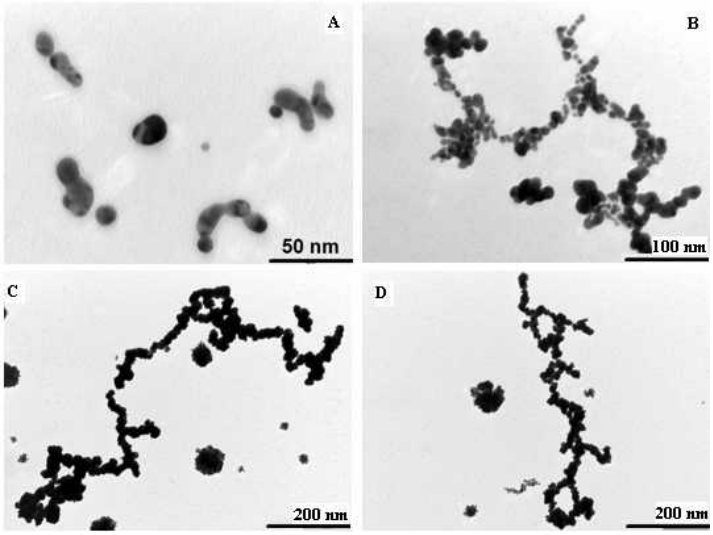

Fig16 AD: TEM images of of lysine-GNP nanostructures at ***A***) 15 min **B**) 8h ***C, D***) 24h after synthesis TEM microscopy shows that immediately after preparation the the 'peanut-shape' are formed by L-Lysine capping gold nanoparticle (***Fig. 16 A***).

As well known, amine-group has a lower affinity for {111} facet compared to other facets Consequently, the uncovered {111} facet is available for nanoparticles fusion which leads to gold nanochains formation. The chain-like structures were generally observed after longer reaction time (24 hours) due to connection between peanut-shape particles with other nanoparticles from solution (***Fig16 CD***).

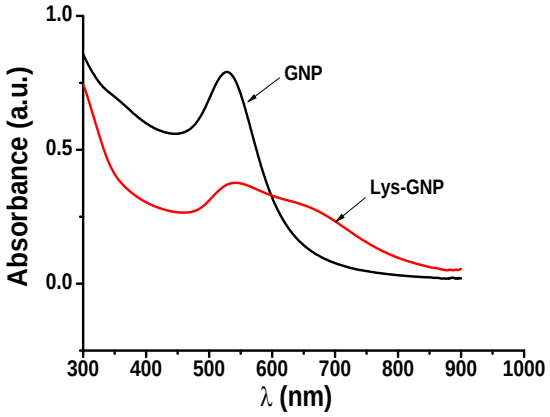

***Fig17*.** UV-VIS spectrum of gold nanoparticles (black) compared to that of lysine functionalized nanoparticles (red)

Fig17 shows the absorption spectra of citrate capped nanoparticles, respectively lysine capped nanoparticles. Since citrate capped nanoparticles are highly dispersed in solution, the spectrum is characterized by a single SRP band, at around 530 nm (transverse surface plasmon resonance band). In contrast, lysine capped nanoparticles exhibit two absoption bands, at 530 nm respectively 680 nm. The appearance of the second band (longitudinal surface plasmon resonance band) is a clear evidence of the linear assembly of gold nanoparticles in solution.

I.1.2.2 Preparation and characterization of 1D nanostructures based- aspartate GNP

Asp plays both the role of reducing and capping agent.The α-amine group has the pK_a 9.6 while α-carboxylic groups pK_a 1.8.In this case the amine is positively charged and the carboxylic group dissociates, that means that the COOH groups reduced the nanoparticles and NH_3 capped them together and formed 1D triangular and spheric nanochains. The anisotropy, isotropy and concentration of the solution have a great significant role in the formation of different nanostructure such as: triangle, nanorods, spherical namowires.

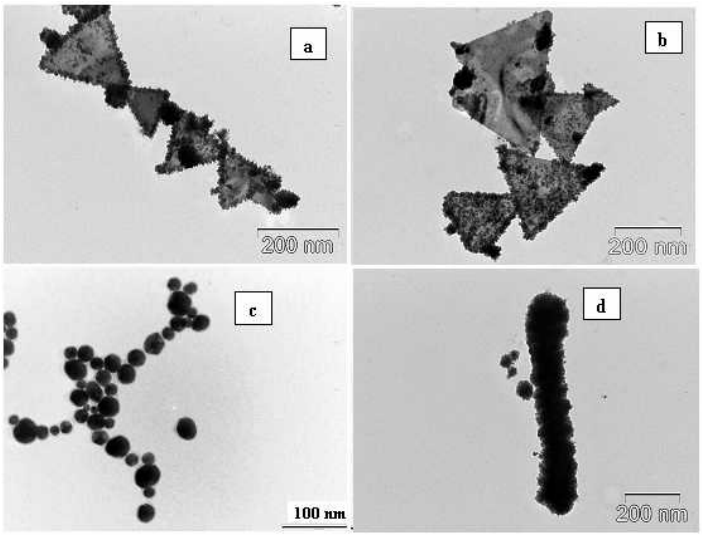

Fig .19 ad: TEM images for different morphologies of L-aspartic-GNP: a, b) report HAuCl4/Acid aspartic-1: 3 after that 9h 24h, c) aspartic HAuCl4/Acid: 1:1 (after 24 h) , d) aspartic HAuCl4/Acid-1: 1.25 (after 24 h)

I.1.3 Two-dimensional nanostructures based on gold nanoparticles- aminoacids

The synthesis of one-dimensional (1D), two-dimensional (2D) and three-dimensional (3D) nanostructures using metallic nanoparticles and biomolecules is a subject of

intensive research, due to their possible applications in microelectronics, optoelectronics, biosensor devices and medicine.[201-205]

I.1.3.2.1 Morphological and optical characterization of 2D nanostructures

The assembly of GNP with amioacids was performed by an exchange of ligands .The ligand used as a stabilizing ligand, citrate, was removed from the surface and gold nanoparticles were assembled with L-lysine, L-cysteineas shown in ***Fig.21 a-c***.

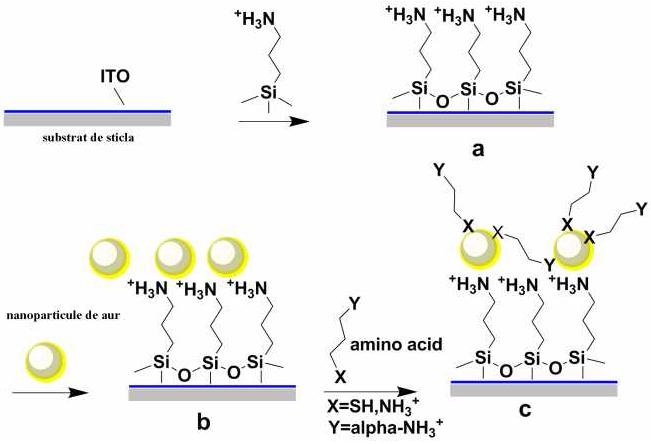

Fig.21 a-c. Chemistry of the attachment of amino-acid to self-assembled AuNP layer: (a) surface silanization with APTMS; (b) addition of gold nanoparticles; (c) linking amino acid (L-lysine or L-cysteine) to AuNP layer

The AFM images showing the AuNP morphology on silanized ITO are presented in Fig.2a. It is interesting to notice that in this case, gold nanoparticles were assembled into large aggregates (size between 40 and 200 nm) which were not in good contact with each other. The poor contact observed between the aggregates (see the arrow) was reflected in a high resistance value, obtained for AuNP/ITO.

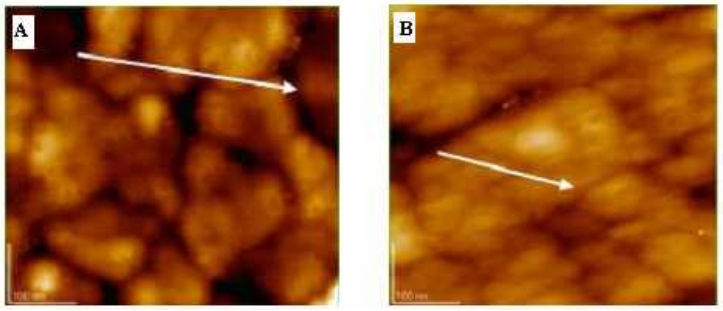

Fig.23 A, B *Tapping™ mode AFM images of* ***A****)AuNP layer on silanized ITO* ***B****) L-lysine/AuNP layer on silanized ITO; scale bar 100 nm*

I.1.3.2.2 Electrical characterization of 2D nanostructures

The potential use of 2Dnanostructures can be found in electronic and biosensors; their electrical haracterization is needed. The electrical properties of AuNP layer assembled on silanized ITO were investigated by I-V measurements (***Fig.25***).

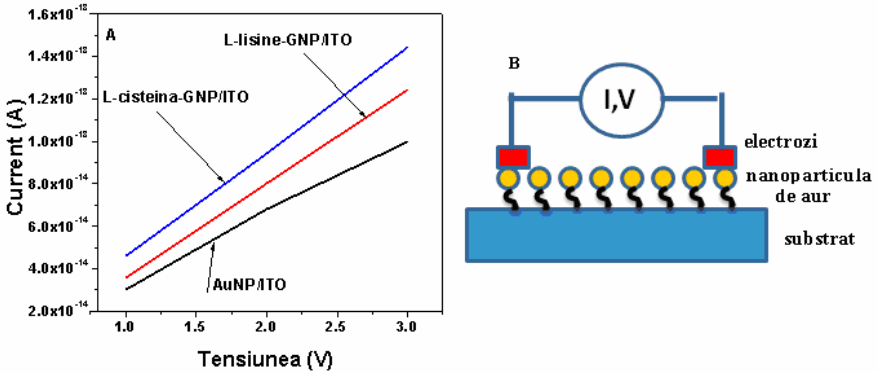

Fig.25*. I-V characteristics of: AuNP, L-Lysine-AuNP and L-cysteine-AuNP layers on silanized ITO substrate (a), and the design of the setup used for this study (b)*

The electrical resistance of gold nanoparticles layer determined from I-V measurements was very high ($2.8x10^{13}$ Ω). After linking L-lysine or L-cysteine to the nanoparticles surface, a change in morphology occurred. The interparticle distance decreased, which consequently leads to a slight decrease of the electrical resistance ($2 x10^{13}$ Ω).

I.2 Functionalization of gold nanoparticles with proteins

In this chapter are presented the interaction of gold nanoparticles with proteins, namely with human serum albumin (HSA Human Serum Albumin-), bovine serum albumin (BSA Bovine Serum Albumin-) and collagen. I highlighted the main factors that affect the linkage protein-GNP: the method choosed for preparation of the nanoparticles (stabilizing agent, auric salt nature, nature reducătorului) and the pH effect.

I.2.1 Functionalization of gold nanoparticles with collagen

Collagen (Coll) is a major component of connective tissue and is one of the most commonly used biomaterials in tissue-engineering given its excellent biocompatibility, biointegration and biodegradability. To improve its mechanical stability and to decrease its biodegradation rate, several cross-linking procedures—including reactions with glutaraldehyde, isocyanates, epoxides, and bis imidates, as well as thermal treatment, UV or gamma-ray irradiation, and photo-oxidation—have been developed and proposed. Using GNPs as a cross- linking agent in collagen gels allows for easy incorporation of biomolecules (growth factors, cell adhesion molecule s and peptides) through their biochemical immobilization at the gold surface without additional alteration of the collagen structure. [208] At present very little is known about the behavior of stem cells proliferation properties over nanostructural biomaterials or GNPs[209] and the results presented in this report could be used for the development of tissue engineering platforms for the regeneration of organs and tissues.

I.2.1.1 Influence of pH and reducing agents on collagen functionalization

The metallization process of collagen used and developed during this study is presented in ***Fig.*35** A change of color occurred, and the solution turned from transparent to pink.

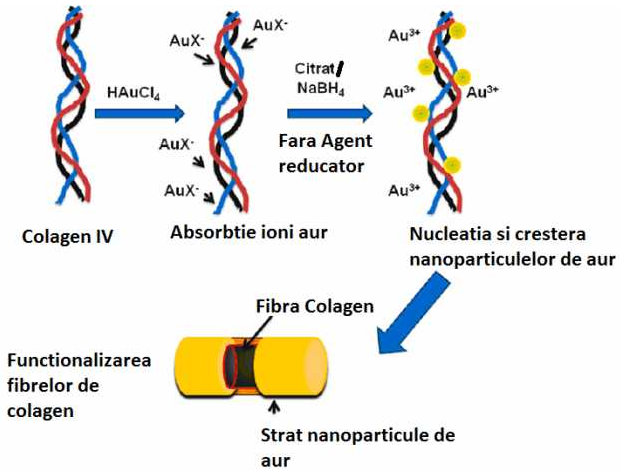

***Fig.*35** Schematic for the collagen gold coating process, resulting in collagen nanofibers coated with thin layers of gold (GCNF).

When no reducing agent was added, Au(III) was reduced to Au(0) by the functional groups that have reduction capabilities and are present on the collagen surface. This process occurred only in acidic medium The pH of the solution influences the nucleation and growth of Au crystals on the collagen substrate. Recently, GNPs of various sizes have been synthesized by the reduction of $HAuCl^-$ ions on the substrate by different kinds of reducing agents at various pH ranges.[210]

By using the above-mentioned method, we successfully generated gold-coated collagen nanofibers (GCNF) with various lengths by the simple manipulation of the assembly conditions. [211] Increasing the pH from 3.5 to 11 and decreasing the speed of mixing resulted in molecular aggregates that have the ability to link end-to-end to create different nanofiber lengths and diameters. Short nanofibers, having a homogenous sedimentation, were produced with $HAuCl_4$: Collagen: sodium citrate ratio of 1:1:1 (wt/wt) at pH=3.5 by mixing the solution at high speed to increase turbulence and exposure (***Fig.*35a**). Under the same conditions but with increasing pH (pH=5.5-6.5), the collagen molecules form more highly-ordered structures, as presented in ***Fig.*35b, c**. Under neutral and slightly alkaline conditions (pH 7.0–9.0), we obtained longer nanofibers but with a non-homogenous surface gold coating distribution (***Fig.*35 d, e**). In more alkaline medium, slightly distorted nanofibers were obtained (**Figure 2 f**).

Nanofibers formed by using NaBH4 (***Fig.*35 g, h**) as the reducing agent have almost the same length (1.2μm -1.8 μm) as in the case of sodium citrate (***Fig.*35 b,c**), but they differ in diameter: width 60-65 nm for citrate and 20-27 nm for borohydride. In the absence of a reducing agent and acidic pH=5.5, long metallized nanofibers (length: 1 μm-2 μm, width 30-35 nm) formed (***Fig.*35 i)**. The adsorption is higher in the acidic region (pH 3.5–5.5), indicating that slightly acidic conditions favor the reduction of Au(III) ions.

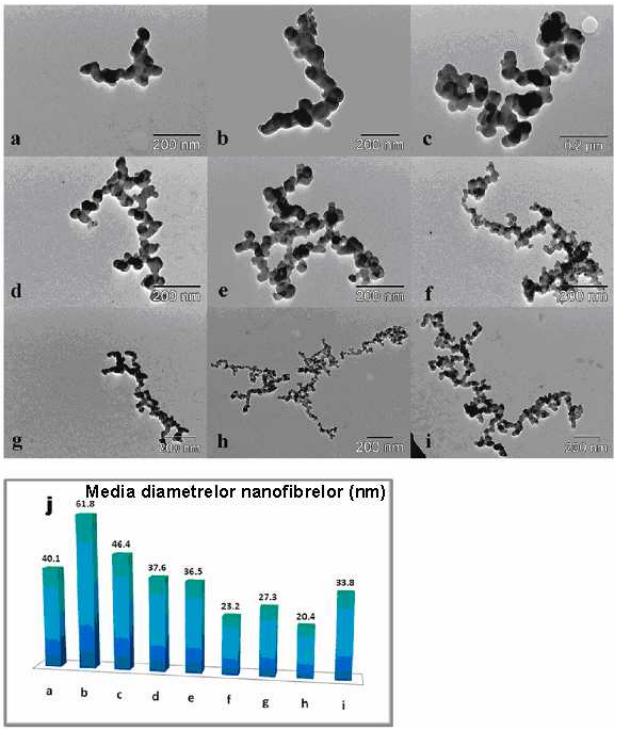

***Fig.*35**: Transmission Electron Microscopy (TEM) images along with the histogram of the size distribution of collagen-based gold nanofibers. TEM images of collagen-based gold nanoparticles with and without reducing agent at different pH: (**a**) sodium citrate-short nanofibers at pH=3.5; (**b**) medium nanofibers pH=5.5; (**c**), (**d**), **(e**), (**f**) longer nanofibers at pH=6.5, pH=7, pH=9, pH=11; No reducing Agent: $NaBH_4$ long nanowires at pH=5.5 (**g**), and longer nanowires at pH=7 (**h**); (**j**) the representative histogram of gold nanofibers obtained under different conditions.

I.2.2 Physical-chemical characterization of functionalized collagen fibers

The collagen Nanofibres obtained after the above-mentioned conditions were characterized by UV-VIS spectroscopy techniques FTIR, transmission electronic microscopy (TEM) and electrical conductivity.

UV-VIS spectroscopy confirmed the formation and adsorption of gold ions over the surface of the collagen macromolecules; this process was monitored after 30 min and 24h, respectively.

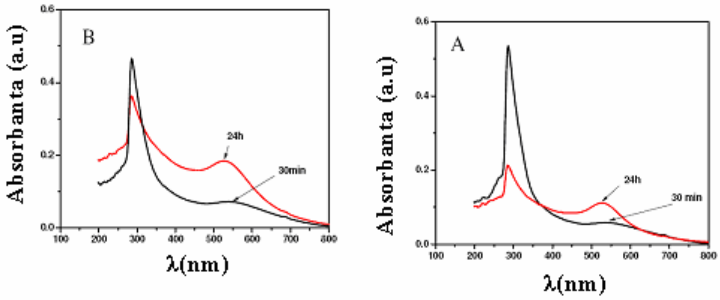

Fig.36A, B. UV-VIS absorption spectrum of collagen metallic structures at pH = 5 monitored after 30 min and 24 h (A) when NaBH4 was used as reducing (B) when not used any decrease.

UV-Vis spectroscopy is an excellent method for studying GCNF formation and their agglomeration. During aggregation, the shifting and broadening of surface plasmonic bands were observed to occur. Here, the nanofiber solution shows broad adsorption bands at around 300 nm and adsorption peaks centering between 520-540 nm. This adsorption peak is characteristic of gold metal nanostructures, and its intensity increases with time, indicating the formation of nanostructures attached to collagen. The broad absorption bands around 300 nm suggest the existence of $HAuCl_4$ in solution. Comparing cases **a** and **b** it can be concluded that, when the reducing agent is added, nucleation and growth occur more quickly; the nanoparticles are more homogenously distributed, and no agglomeration is observed. In the case presented in (***Fig.36 B***) with no reduction agent used, the reduction occurs in time, and the broad peak around 520-540 nm suggests that the particles tend to agglomerate

The interaction between gold nanoparticles and collagen macromolecules indicated by TEM and UV-VIS spectroscopy was also confirmed by FTIR analysis, as shown in ***Fig. 37***

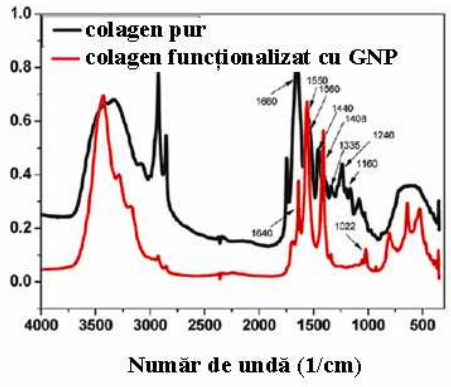

Fig.37 *FTIR spectrum of collagen structures (black) compared to that of metalized collagen (red)*

Some FTIR characteristic peaks for pure collagen were found to have changed their positions while others disappeared when GNPs were attached to the collagen structure. The upper region 3750-2750 cm^{-1} changed dramatically. The C-H stretching corresponding peaks from 2700-3000 cm^{-1} disappeared, and the single band at 3375 cm^{-1} arose after metal absorption. This band is given by the stretching vibrations of the NH^{3+} groups that are involved in electrostatic bonds with gold. Moreover, the absence of C-H stretching bands, in contrast with their presence in pure collagen, is due to the chain length of collagen and its molecules' parallel orientation on the gold surface. The molecules pack to densities sufficient to form high-quality barriers for both electron- and ion-transfer processes.[32] Furthermore, the amide I absorption, characteristic of C=O stretching vibrations, appears with a position changed from 1660 cm-1 to 1640 cm^{-1}; Amide II absorption, N–H bending vibrations, and C–N stretching vibrations shifted from 1550 cm^{-1} to 1560 cm^{-1}; Amide III, C–N stretching, and N–H in plane bending shifted from 1240 cm^{-1} to 1022 cm^{-1} because of their interactions with the GCNF surfaces. Also, the characteristic vibrations of the COO^- groups or C-O vibrations of alcohols from the hydroxyprolyne or glycosidic side chain shifted from 1440 cm^{-1} to 1408 cm^{-1}. In this case, the peak intensities dramatically decreased along with band broadening.

To demonstrate their potential applications as an electrically conductive substrate for placental-derived mesenchymal stem cell differentiation, we investigated their electrical properties by using I-V measurements. The continuous coverage of the collagen fibers with gold metal particles shown by transmission electron microscopy suggests that they are electrically conductive. The current-voltage (I-V) curves of the gold metal-coated collagen substrate with its measured electrical resistance value of 2.36 MΩ are presented in ***Fig.38***

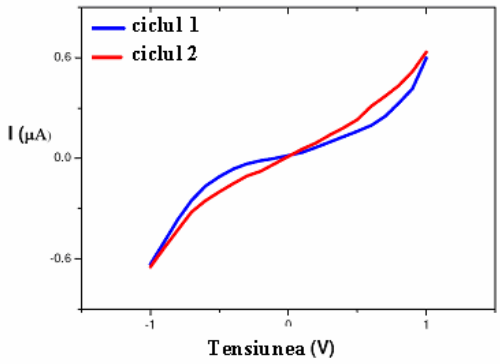

Fig.38 Current-voltage curves (IV)of metalized collagen fiber

.The I–V sweeps (cycle 1, 2) do not present a typical ohmic character, but instead present symmetric current plateaus centered upon zero voltage, indicative of electron-tunneling barriers. Because the nanofibers were generated by chemical reaction, there are many grain boundaries that hinder the current flow. This behavior is not surprising, and the electron conduction takes place through hopping between the adjacent domains.[33] Repetitive cycling of the device could reduce these effects until almost purely ohmic behavior is obtained. In our case, after 15 cycles of I–V scans, an ohmic behavior with a resistivity value estimated to be 4×10^{-5} m was measured. It is believed that this cycling process anneals the metal grains and improves the current transport through the substrate.

I.2.3 Applications of collagen functionalized gold nanoparticles

I examined the ability of placental-derived MSCs to differentiate into cardiomyocyte and neuronal lineages when cultivated *in vitro* on different substrates: *e.g.*, none (ctrl), collagen only (coll), and metal-coated collagen nanofibers GCNF substrates noted as MC. The metal-absorbed collagen substrates proved to be the most effective.

Moreover, we demonstrated that the spatial arrangement of collagen along with the potential of GCNFs to deliver electrical stimulation induce a faster neuronal and cardiac differentiation of the stem cells, when the metal-absorbed collagen substrate is exposed to electrical stimulation.

When cells were cultured over the MC substrates, few of the substrate fibers were observed to be internalized during the first few hours. MSCs have the capacity to bind and uptake collagen through their uPAR-associated proteins uPARAP/Endo180 with the FnII domain being responsible for the binding and uptake. The endocytosis uptake is followed by progressive intracellular accumulation, especially in the perinuclear region, after a few weeks, with no signs of cytotoxicity. ***Fig.41*** demonstrates the desired biocompatibility of the gold metal-coated collagen substrate with the stem cells, showing the internalization of the substrate's component GCNF inside the cells

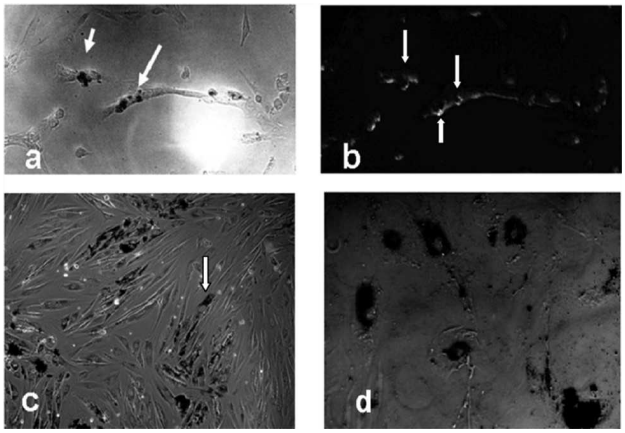

Fig.41. Chorion-derived MSC cultivated on gold-coated collagen (GCNF) substrate (MC) showing intracellular intake of the metallized fibers; 3 days of cultivation-phase contrast image (a) and dark field image (b) (magnification X200); 13 days of cultivation in presence of myocardial differentiation medium and after (c) 1 month of cultivation with neuronal differentiation medium; (d) (phase contrast image magnification X400).

To assess the biocompatibility of adult stem cells with various substrates, we used the MTT assay and FDA fluorometric technique. Chorion-derived MSCs (Ch-MSC) were

cultivated on substrates under different conditions: 1- with complete stem cell medium that maintains the cells in the undifferentiated state; 2- cells exposed to neuronal differentiation medium; and 3- cells treated with one dose of 5AZA for 24 hours. The results of the MTT viability and proliferation test are presented in ***Fig.42A-D.***

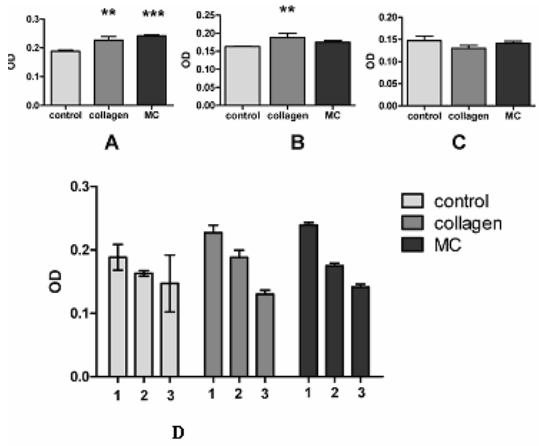

Testul MTT pentru celulele MSC in raport cu substratul si protocolul de diferentiere:
1. mediu de celule stem
2.mediu de diferentiere neuronala
3. mediu de diferentiere miocardica

Fig.42A-D.MTT proliferation assay for Ch-MSCs cultivated for 7 days in undifferentiated state (control) (A), in presence of neuronal differentiation medium (B) and in the presence of myocardial differentiation medium (C), without substrate as control in comparison with substrates: collagen (Coll) and gold-coated collagen (MC). Two-way ANOVA Bonferroni post-test collagen and MC substrates (D).

When no differentiation medium was used, one–way ANOVA analysis (set at $p < 0.05$.) showed a statistically significant increase in proliferation for cells cultivated on collagen and gold-coated collagen (MC) substrate, compared to the control without substrate (***Fig.42*A).** When cells were cultivated for neuronal differentiation, a more sustained statistically significant proliferation resulted in the case of collagen **(*Fig.42*B).** We note that the progressive decrease in cell number in the case of gold metal-coated collagen (MC) suggests the initiation of the differentiation process. No significant differences were observed in the case of myocardial differentiation **(*Fig.42*C).**

We also performed a cell viability analysis using a two-way ANOVA Bonferroni posttest comparison of grouped data in relationship to the substrates (statistical significance was set at $p < 0.05$). We observed no significant difference between samples **(*Fig.42*D)** in all three conditions of cultivation (1- with complete stem cell medium that maintains the cells in undifferentiated state; 2- cells exposed to neuronal differentiation medium; and 3- cells treated with one dose of 5AZA for 24 hours).

Cells cultivated on CM substrate process an accelerated differentiation, the cells developed more characteristic morphologic features for neuronal lineage in the presence of gold-coated collagen substrates-MC (***Fig.43E,F***).

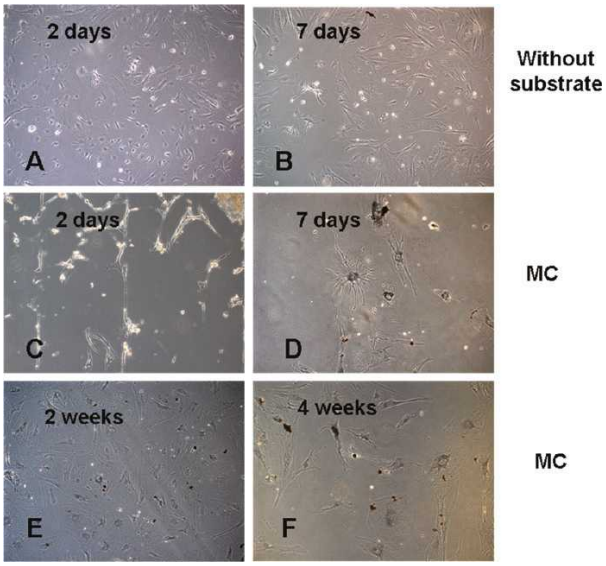

Placental MSCs grown on MC substrates responded in 1-2 days to neuronal induction medium by generating cells bearing neuronal-like extensions (***Fig.43*** **C, D**) and neuronal-like morphologies when compared with cells cultivated without substrate (control) (***Fig.43*****A, B**). Ch-MSCs cultivated on MC substrates formed of GCNF had a characteristic morphology represented by intracellular uptake of gold-adsorbed collagen with an increased level at 2 and 4 weeks (***Fig.43*****E, F**).

To assess neuronal differentiation of placental-derived MSCs, we performed immunohystochemical staining of the samples (***Fig.45 A-I***.). We observed the expression of GFAP and neurofilament (NF) differentiation markers: GFAP was expressed in cells cultivated without substrate (***Fig.45C***) and on all substrates used (collagen, gold metal-coated collagen) (***Fig.45* F, I**). Expression of neurofilament (NF) was also observed in differentiated cells on all substrates: collagen and MC, with a greater staining for some cells with a neural-like morphology (***Fig.45* B,E,H**). Additionally, GCNF substrates induced dramatic changes in cell morphology with a strong expression of NF (***Fig.45* H**), with accumulation of GNPs in the perinuclear spaces and in neural-like extensions. Moreover, characteristic alignment of cells was observed for those cultivated on collagen and gold metal-absorbed collagen suggesting that the presence of collagen induced orientation of the cells in the same direction (***Fig.45* A,D,G**)

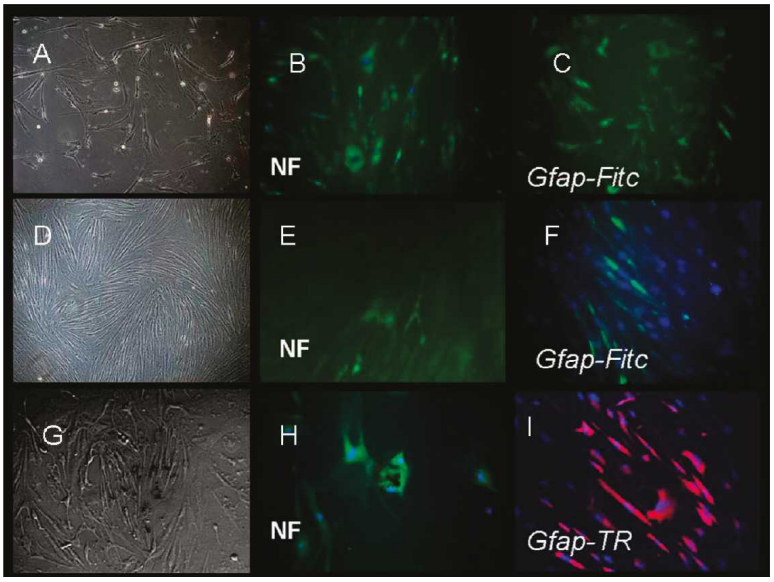

It seems that the combination of gold nanoparticles with collagen is also the most favorable substrate for a more advanced differentiated state of placental MSCs in this

experiment. There are some *in vitro* studies regarding neuronal differentiation, neuronal migration and expansion in the presence of components of ECM such as collagen, fibronectin, laminin, or matrigel.[218-220]

Another aim of this study was to investigate the cardiomyogenic potential of placental-derived MSCs *in vitro* using different substrates: collagen and GCNFs. The controls were cultivated without substrate. To induce cardiomyogenic differentiation, cells were cultivated in standard stem cell medium for 4 weeks and treated with the demethylating agent 5-azacytidine (10 µM) for 24 h with 1 cycle of exposure/week (in total-4 cycles of 5-AZA). The cardiac phenotype was assessed by immunostaining (***Fig.46 A-F***) with cardiac marker expression after 4 weeks of myocardial differentiation induction: early cardiac specific homeobox protein Nkx 2.5, atrial natriuretic peptide cardiac hormone (ANP), and with phalliodin for the rearrangement of filamentous actin (actin F). Ch-MSC adopted a ball-like or polygonal morphology—a morphology consistent with myotube-forming cells as reported by Martin-Rendon *et al.* [221] This cellular morphology could be explained by the remodeling and assembly of the myofibrils when cells are exposed to an actin-induced stress resulting in the change from a fiber-like to a polygonal shape, morphological aspects more clearly observed in ***Fig.46D,E.***

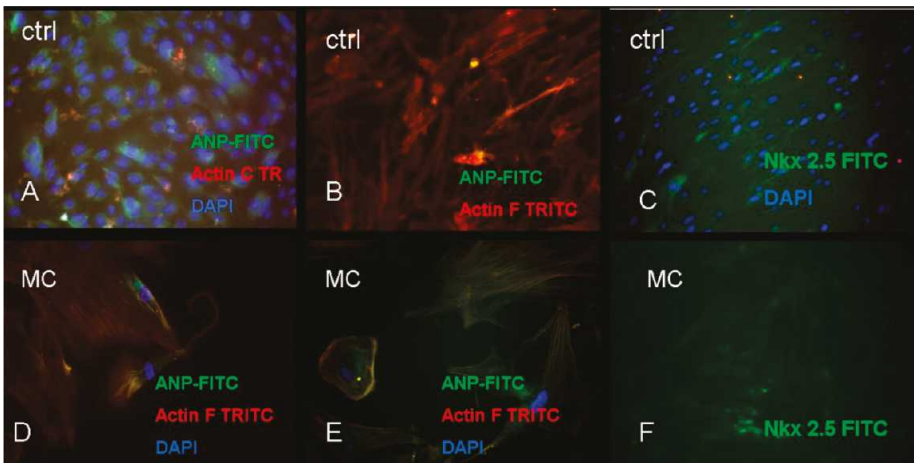

Fig.46D

Immunohistochemical analysis revealed that induced cells were positive for Nkx

2.5 even in the absence of a substrate (***Fig.46 C***). The characteristic stick-like morphology of cells cultivated without substrate was observed after actin-F phalloidin staining (***Fig.46* B,C**). The cardiogenic homeodomain factor Nkx-2.5 cooperates with GATA-4, expressed in early cardiac progenitor cells, to activate the α cardiac actin.Cultivation of Ch-MSCs in the presence of gold metal-absorbed collagen shows the intranuclear localization of Nkx 2.5 (***Fig.46 F***)

Myocardial induced cells cultivated on gold metal-absorbed collagen were strongly positive for ANP expression in comparison with control cells, despite a shorter cultivation period of 3 weeks (***Fig.47A,B***).

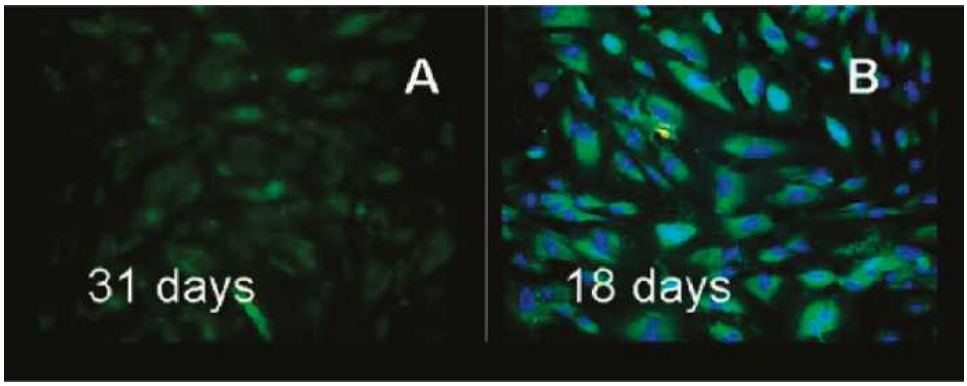

Fig.47A,B

The effect of 5-Azacytidine may not be specific because it induces uncontrolled myogenic speciation and changes in phenotype by activating a large number of genes. Moreover, isolated treatment with 5-azacytidine may not be sufficient to re-program MSCs to give rise to enough cardiomyocytes for cardiac repair. Other strategies, such as the development of constructs that show both mechanical stimulation in addition to biochemical and electrical stimuli, may be necessary to obtain a fully functional, differentiated cardiac phenotype. GCNF substrates attain all three of these characteristics.

Additionally, we exposed placental-derived MSCs to electrical stimulation, provided by a clinically used pacemaker, with concomitant treatment of cells with neuronal and cardiomyocyte differentiation induction media. Electrical stimulation with the neuronal differentiation protocol accelerated the acquisition of neural-like morphology (Figure 10) even after 24 hours of electrical stimulation, ***Fig.48A-F.***

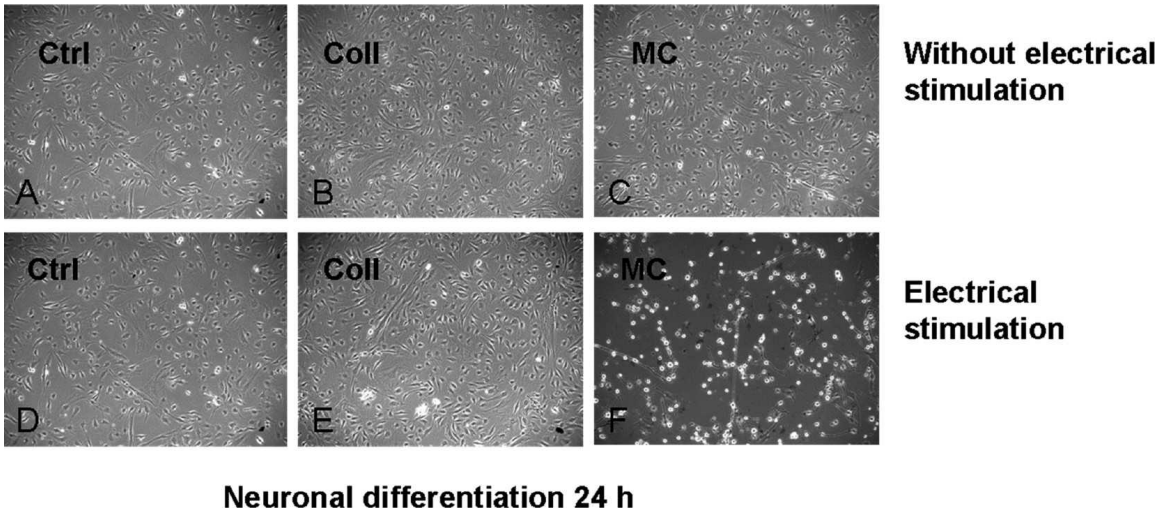

Fig.48A-F

Placental MSCs exposed to an electrical field displayed rapid morphological changes and expressed cardiac specific genes (troponin I, Nkx2.5, and GATA-4 analyzed by Reverse Transcription-PCR; data not shown here) (***Fig.49A-D.***)

.

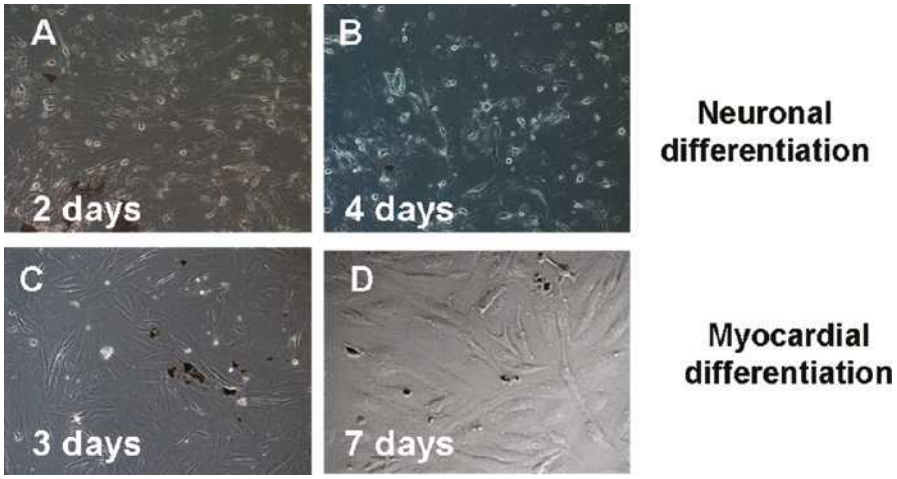

Fig.49A-D,

I.4.1 Functionalization of gold nanoparticles with temozolomide

Temozolomide is an oral alkylating agent used for the treatment of malignant tumors of neuroendocrin origin, including high-grade gliomas and melanomas. This drug has the ability to alkylate or methylate DNA most often at the N-7 or 0-6 positions of guanine residues, thus damaging DNA and triggering apoptosis of the cancer cell. By binding the gold structure to the drug, I hope to improve the treatment of WHO grade III and IV CNS tumors owing to the increased efficacy of the newly formed compound. The dimer formed by GNPs and Temozolomide has been shown to have an increased uptake by the cancerous tissue in comparison with normal ones because of the surrounding edema and increased neovascularisation, but also because of its increased anticancer properties in comparison with the current standard-of-care, as shown in chapter ***I.4.4***

Methods

The simple method described in chapter **I.1.2.2** provides large-scale production of GNPs-L-Asp nanostructure that is required as intermediates in the preparation of the target delivery vectors. Onto our previously GNPs-L-Asp nanostructure solution (10 ml) was added 200 µl TMZ (50 µl/ml) and mixed for 1 hour. The resulted compound was centrifuged three times at 15000 rpm for 1 hour washed with milly Q water and redispersed in PBS.

The formation GNPs-L-Aspartate-TMZ delivery vector is schematically ilustrated in ***Fig.56.A,B***

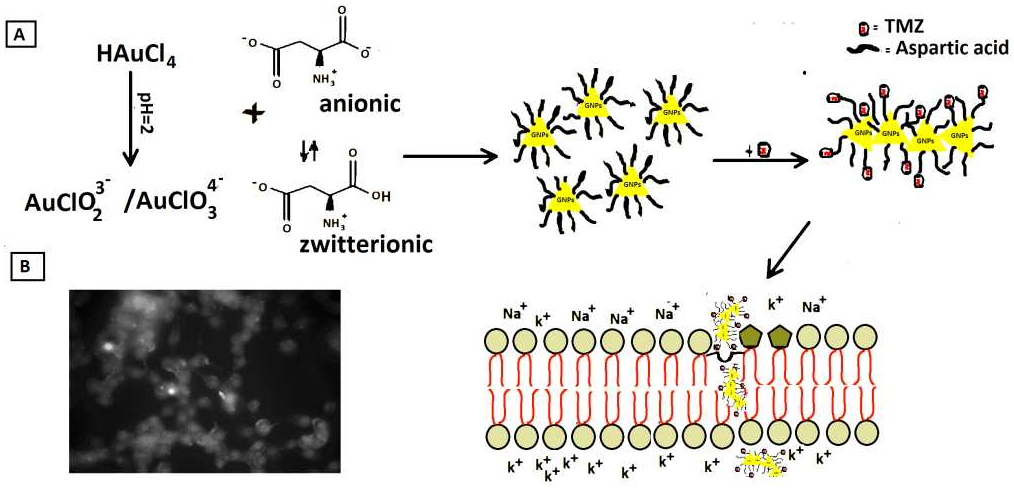

Fig.56.A,B - *Drug delivery system formation. A- Formation of the GNPs-L-Asp-TMZ Nanostructures B-Uptake of the system into glioblastoma stem cells.*

First , I synthsised the carrier, gold nanostructure. I reducDe HAuCl4 in strong acidic media, pH=2,in the presence of L-Aspartate molecules. Mixed chloro-hydroxo complexes ($AuCl_2O_2^{-3}$ or $AuClO_3^{4-}$) are present around L-aspartic molecules wich reduce the gold salt to gold nanoparticle and stabilize them into 1D triangle nanostrucutres. Further these nanostructures have been used as building blocks for to the formation of nanostructure the desired delivey vector, GNPs-L-Asp-TMZ has been obtained. As shown in Scheme 1, TMZ was conjugated to GNPs-Laspartate-TMZ by forming electrostatic bonds between TMZ and aspartate molecules. The formation was confirmed by electron microscopy (TEM) vibrational spectroscopy (FTIR) and X-ray Photoelectron Spectroscopy (XPS).TEM analysis along with the diameter histogram are presented in ***Fig.57a-c.***

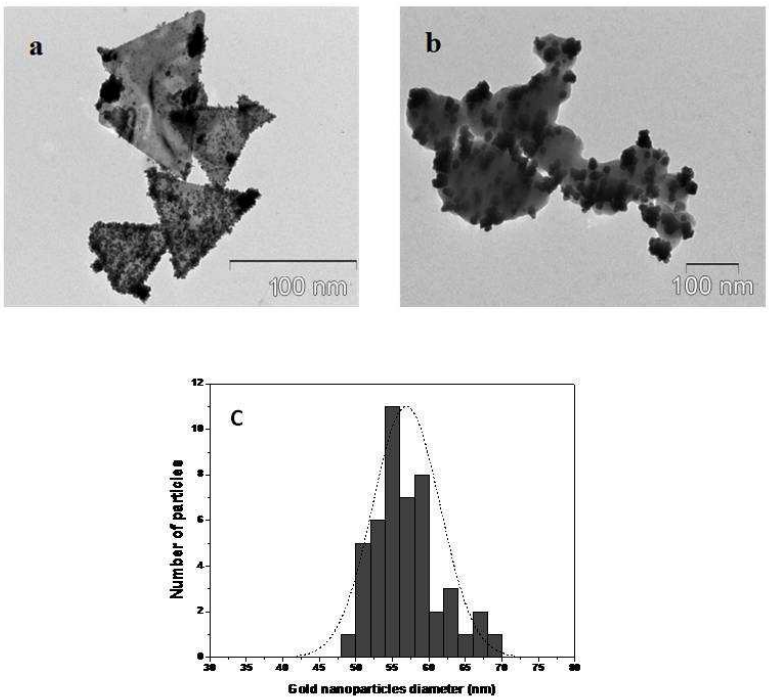

Fig.57.a- c. *TEM images of a)GNPs-L-Aspartate nanostructure (b) GNPs-L-Aspartate-TMZ delivery system (c)*a representative size distribution histogram of the gold nanoparticles

The images confirm the formation of the nanostructure and their triangular shape. The length of the chains ranged from hundreds of nm to few micrometers, having a medium diameter of **55 nm.(** ***Fig.57.a***). A typically image showing the drug delivery system is presented in ***Fig.57. b.*** A thin shell, which most probably is the TMZ drug, covers the nanostructure surface. It is interesting to notice that, after the coupling, no secundary effects such as nanoparticle aggregation appeared even after 1year time from their preparation

In order to understand the TMZ-GNPs system, vibrational spectroscopy (FTIR) was utilized.

The FTIR spectra is presented in ***Fig.58***

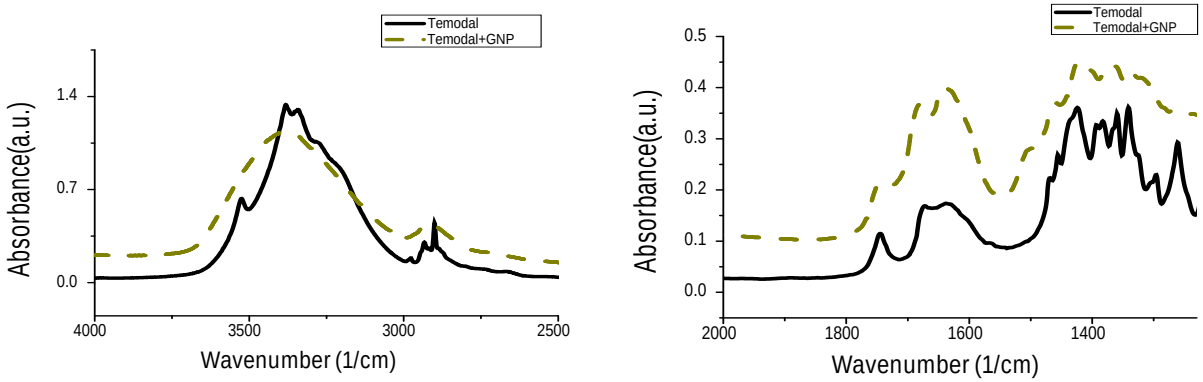

Fig.58 FTIR spectra of (a) pure TMZ and (b) TMZ–GNP-L-Aspartate

In the upper side FTIR spectrum of pure TMZ has three broad bands at 3339, 3381 and 3526 cm^{-1} given by the stretching vibration modes of NH2 and OH, while the two bands around 2935 cm^{-1} and 2899 cm^{-1} were related to the stretching vibrations of the aliphatic methylene groups. After interaction with gold two single bands appeare, in this region: one at 3389 cm^{-1} from the streaching vibration of NH3+ groups and other at 2934 cm^{-1} from the vibration of C-H and CH_3.This change is due to the electrostatic interaction of these groups with gold nanoparticles.

In the middle of the spectrum at 1746 cm^{-1} is the four member ring from ketones band wich is simillare through that of pure MTZ but more intense due to the presence of gold in the structure. The amine I is indirect influenced by the NH_2-nanostructure linkage and has a peak at 1682 cm^{-1}, in the pure MTZ appears at 1672 cm^{-1}. There are not similarity between the FTIR spectrum of pure TMZ and the one of the TMZ–GNPs sample, (all peaks are rounded, shifted) suggesting that between theTMZ molecules and gold nanostructure strong electrostatic interections occured

I.4.2. Functionalization of gold nanoparticles with cisplatin, doxorubicin and capecitabine

The aim of the current study was to evaluate *in vitro* the antitumor efficacy of gold nanoparticles (GNPs) conjugated to conventional chemotherapy drugs for liver cancer, this approach based on gold proposes a novel platform therapy with minimal toxicity and increased efficacy profiles for the destruction of hepatic cancer stem cells. [228]

The coupling reaction mechanism is the same as for functionalization with temozolomide, except that in this case the nanoparticles have spherical shape, ***Fig.61***

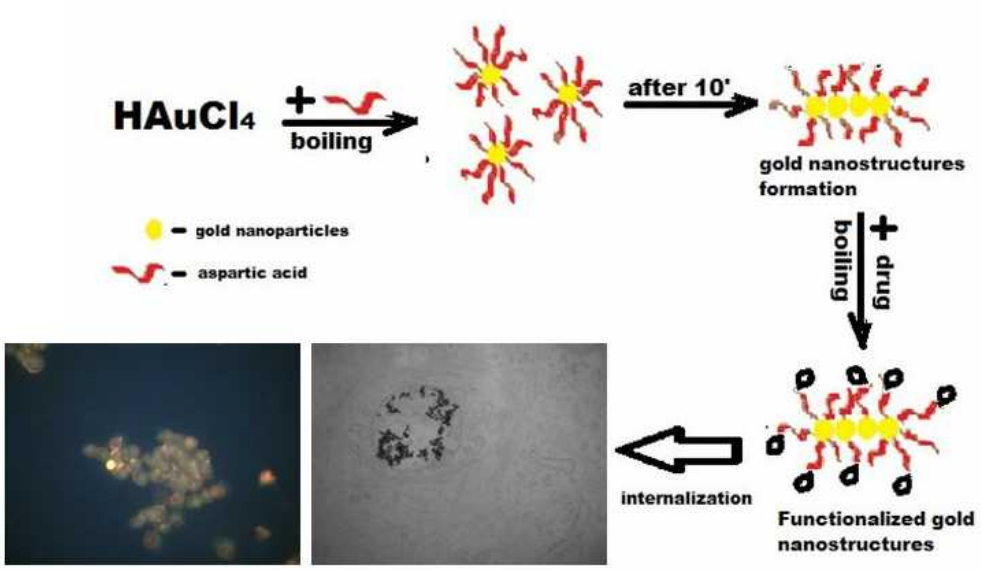

Fig.61. *Mechanism of functionalization of gold nanostructure with the drugs (cisplatin/ capecitabine, and doxorubicin).*

The vectors, doxorubicin-nanocarriers, cisplatin-nanocarriers and capecitabine-nanocarriers, were synthesized by physically adsorption of the drug onto the GNPs-L-Aspartate surfaces. The morphology of the deliveries was revealed by using Transmission electron microscopy (TEM) (***Fig.62a-d***:), where it can be clearly seen that the GNPs-Aspartate structure has been rearranged by the presence of the drugs but it still maintain its nanometric sizes.

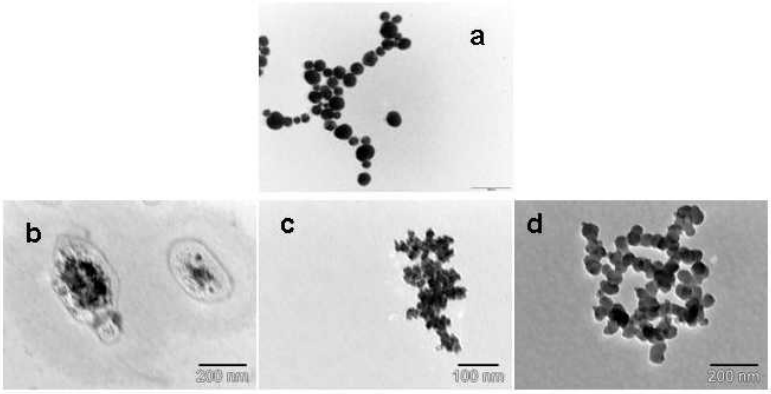

Fig.62a-d TEM images of gold nanostructure (a), gold nanostructure functionalized with cisplatin (b), capecitabine (c), doxorubicin (d).

The noncovalent interaction of the drug to GNPs is dependent on the nature of the drug and its reactive functional groups, which interact with the gold-nanostructures surfaces. FTIR spectroscopy was used to investigate the nature of these groups, and the results are presented in ***Fig.63a-c.***

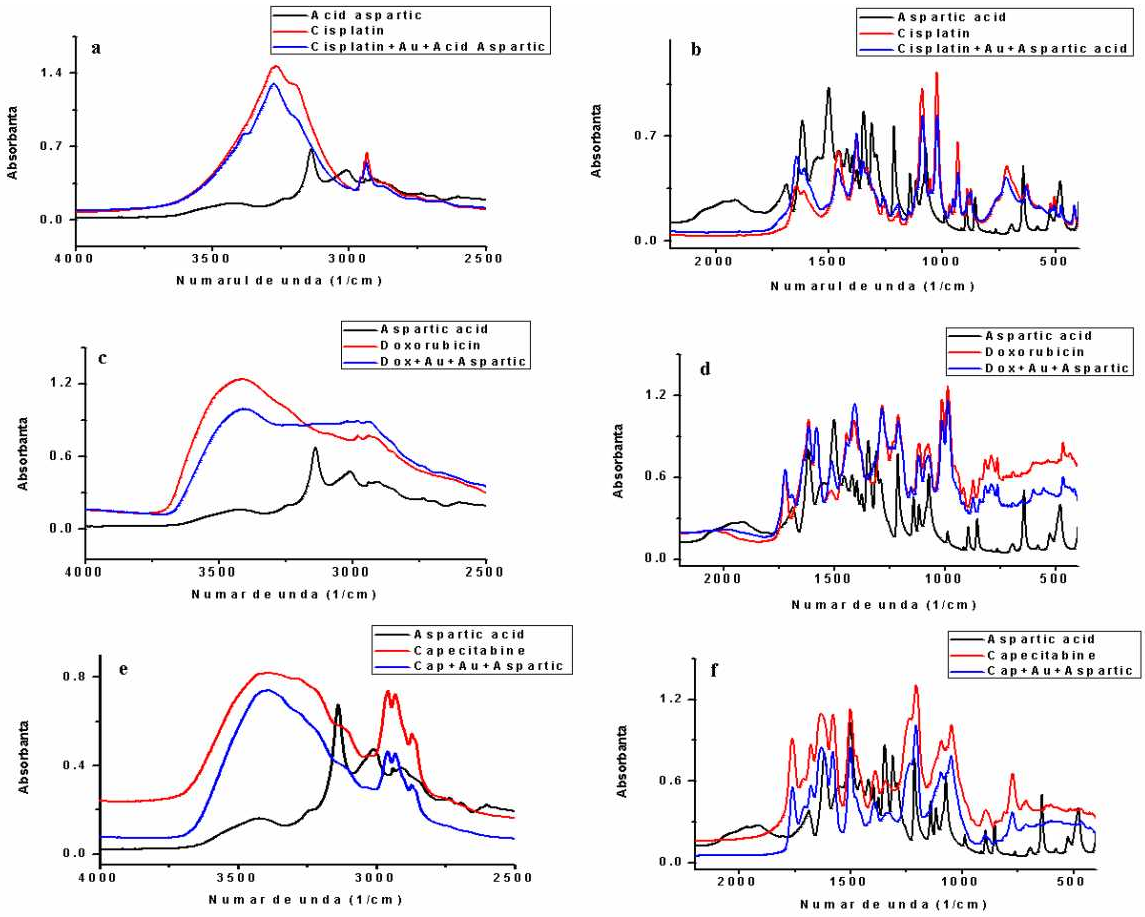

Fig.63a-c.FTIR spectra of gold nanostructures loaded with doxorubicin (a); cisplatin (b), capecitabine (c).

In the case of doxorubicin-loaded carriers (***Fig.63a***) we notice that all the peaks corresponding to the drug functional groups had changed their frequencies, while the phenyl ring peaks remains unchanged, allowing us to conclude that the molecules had attached into the carrier through noncovalent bonds.

The broad band in the range 3200–3700 cm^{-1} is due to the presence of surface-bound $–H_3$-N, –OH functionalities on the nanoparticle surface. This band overlaps with –OH stretching vibration of doxorubicin. The peaks that change the position from to 2980cm^{-1} to 2978 represents the stretching vibration of C-H bonds from the rings. Also, the appearance of hydrogen bonds between doxorubicin and carrier can be attributed to the bending vibration of N-H and stretching vibration of C=O, C^4-H_2, O^4-H. Their corresponding bands appear changed in frequency from 1722 to 1721 cm^{-1}. The band at about 1580 cm^{-1} is related to the ring breathing and appears in the spectrum unmodified. Carboxylate vibrations are visible for doxorubicin in the range of 1400–1445 cm^{-1} together with C–O–C asymmetric stretch at around 1284 cm^{-1}. Also another change in position from 1076 cm^{-1} to 1073 cm^{-1} is attributed to the aliphatic CH_X.

FTIR spectral data were also used to confirm the loading of cisplatin and capecitabine into GNPs-L-Aspartate substrate and is confirmed by the ***Fig.6a,b,e,f*** The bonded cisplatin ***Fig.63a,b*** bands appear shifted but very similar in shape. The asymmetric and symmetric stretching vibration bands of NH_3 overlap in a band located between 3388-3186 cm^{-1}.The asymmetric deformations and the rocking mode in plan and out plane are between 1642-715 cm^{-1}. The region 628-415 cm^{-1} corresponds to symmetric and asymmetric stretching modes of N-Pt. In ***Fig.63e,f*** the characteristic bands that confirm the formation of capecitabine-carrier vector are: at 3385 cm^{-1} and is due to O–H/N–H and gold structural hydroxyls. The band at 1678 cm^{-1} is due to pyrimidine carbonyl stretching vibrations, whereas band at 1757 cm^{-1} represents the urethane carbonyl stretching vibrations. Characteristic bands at 1045 cm^{-1} and 1205 cm^{-1} indicate C–F stretching vibrations as well as the presence of tetrahydrofuran ring.

I.4.3 Applications of functionalized gold nanoparticles –cisplatin/capecitabine /doxorubicin in the treatment of liver cancer

Hepatocellular carcinoma (HCC) is the fifth most common solid tumor worldwide

and the fourth leading cause of cancer-related death, with an estimated death rate of more than 500000 per year [229-230]. Over the past decade, several delivery vehicles have been designed based on different nanomaterials, such as polymers, dendrimers, liposomes, nanotubes and nanorods. [235]

Cellular uptake of the drug

Since the cellular uptake efficiency of drug-loaded GNPs may affect the therapeutic effects, the confirmation of the presence of the cytostatic-loaded nanostructures is very important. Cells incubated with different drug combinations were studied and optical microscopy images (white light microscopy and the correspondent images in fluorescence microscopy at 488 nm) were taken using a Zeiss Axiovert inverted phase microscope. Image acquisition were performed with an AxioCam MRC optical camera. [237] ***Fig.64a,f***.

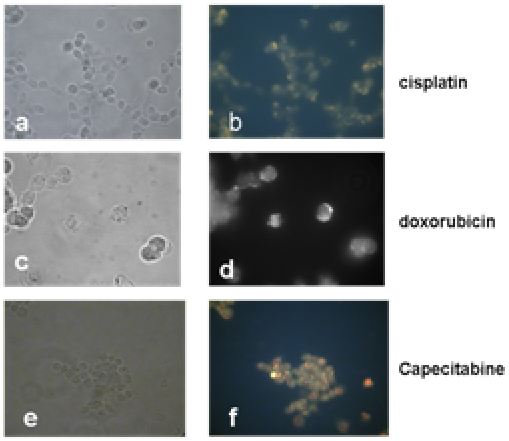

Fig.64a,f Drug-loaded nanoparticle intracellular accumulation on cancer stem cells (X100). Cisplatin (White light microscopy-a and Fluorescence microscopy-b), doxorubicin (White light microscopy-c and Fluorescence microscopy-d), capecitabine (White light microscopy-e and Fluorescence microscopy-f).

In order to elucidate the mechanism of cell killing and to understand the efficiency of the drugs to CSC line, the cells were subsequently inspected by TEM. The TEM micrographs (after 1h of incubation) of the GNPs-drugs nanostructures in CSC cells are presented in

Fig.65a-f

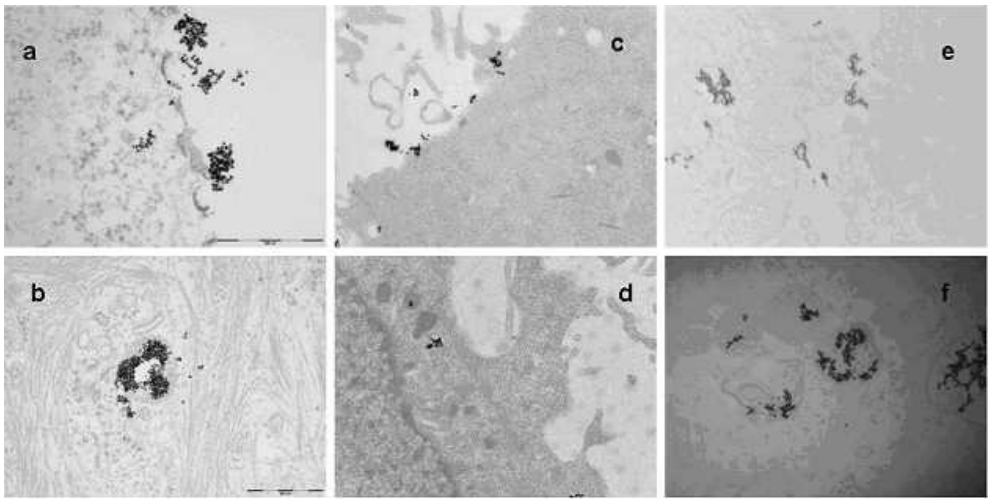

Fig.65a-f TEM micrographs of the drugs in CCS cells after 1 h of incubation: (a, b) GNPs-cisplatin, (c, d) GNPs -capecitabine (e, f) GNPs- doxorubicin.

The route of uptake is a caveolin-dependent endocytosis followed by the release of the conjugated drugs from endosoms/lysosoms into the cytoplasm. Here the reaction between cisplatin/ doxorubicin/capecitabine and DNA occurs.

.

MTT citotoxicity test

CSC and LIV cells grown at subconfluence in 6 well plates were exposed 24 hours to a combination of chemotherapeutic drugs conjugated or unconjugated with GNPs (doxorubicin 0.5μg/ml+ cisplatin of 0.25μg/ml+ capecitabine at 30μg/ml+ Pegylated interferon α-2b 2μg/ml) corresponding to PIAF clinical protocol from Radiobiology and Tumor Biology Department, Ion Chiricuţ ă Oncology Institute, Cluj- Napoca, Romania.

Fig.66 presents the visual differences between CSC, LIV and HepG2 cells, and it can be clearly seen that in the case of HepG2 cells and CSC cells the drug is more efficiently absorbed. If we should analyze the different proliferation rates of the three cell types, we can clearly notice the difference even macroscopically, with great impact in the clinical

management of liver cancer. Such, after chemotherapy, according to our results, the normal liver parenchyma should be able to regenerate and substitute the tumor mass lyzed by the cytostatic regimen due to the surviving normal stem cell population found in the canals of Herig.

Fig.66 Visual observations of the differences in the MTT staining intensity values between CSC, LIV and HepG2 cells; especially in the case of HepG2 cells and CSC cells the drug is more efficiently. The macrosopic visualization observations were confirmed by the MTT optical density values.

The drugs effects on different cells lines can be observed (after 24 hours) macroscopically on the culture flask, a difference also confirmed by the MTT assay. (***Fig.67A-F***).

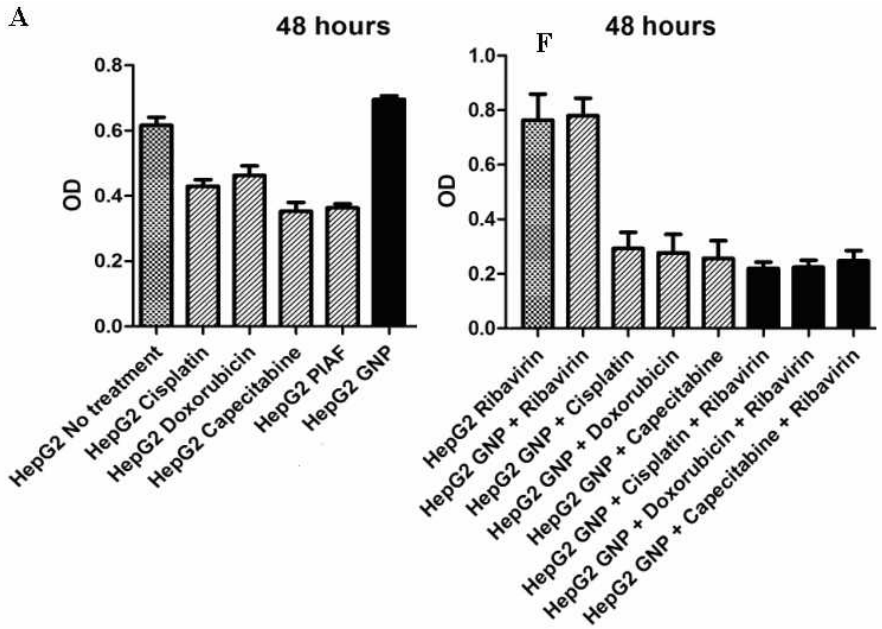

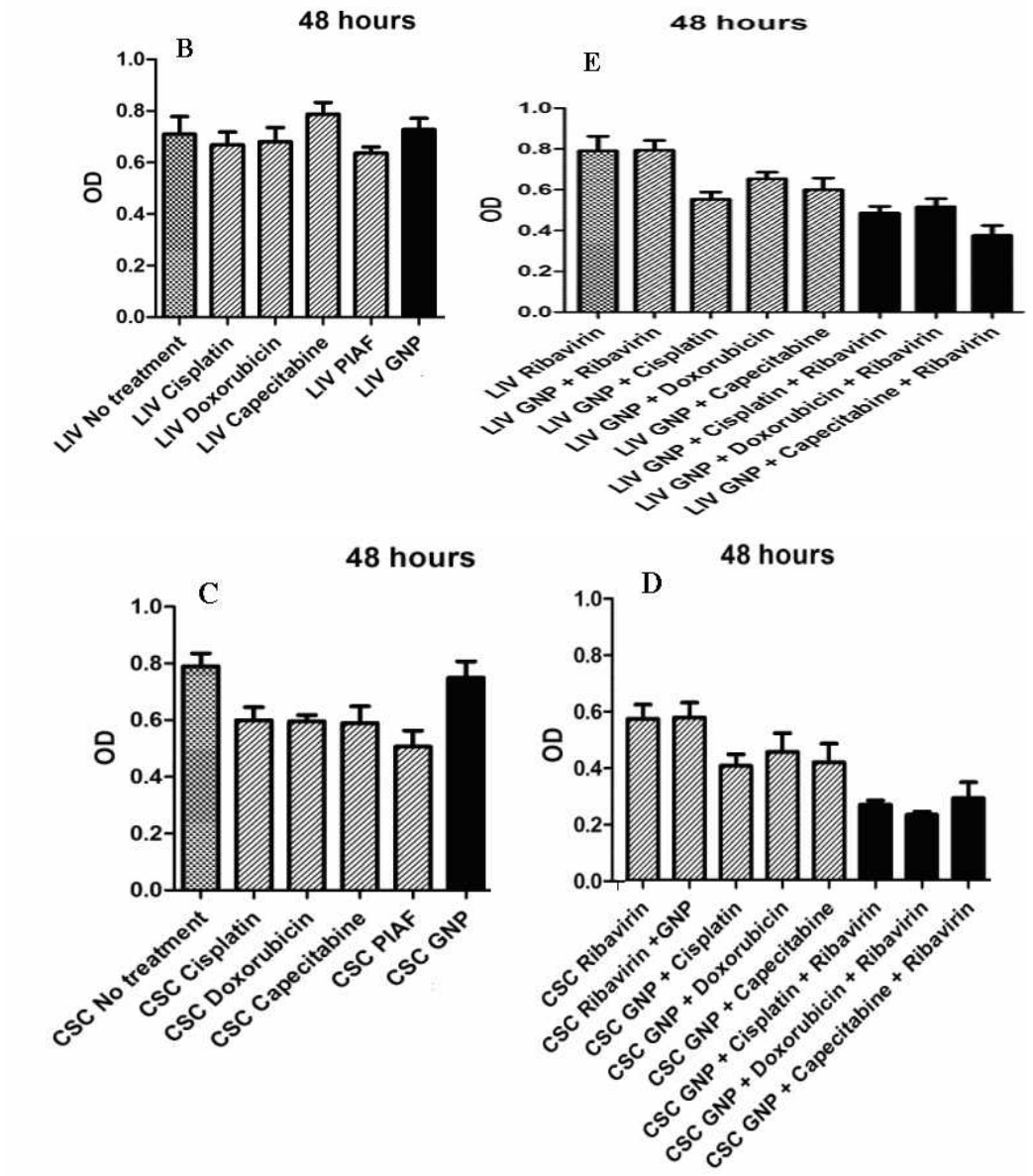

Fig.67A-F Experimental results of the MTT proliferation assay indicating the higher activity of the anticancer drugs in the presence of gold nanomaterials and various cancer lines: (A) HepG2, (B) LIV, (C) CSC, (D) CSC+GNPs, (E) LIV+GNPs, and (F) HepG2+GNPs.

The cytotoxicity level induced by the different drug combinations was measured using the MTT assay, a very commonly used method of evaluating the effects of different substances in cell culture, and which is used to measure the cellular mitochondria function of the cells in the culture dish. The concentrations of the different anticancer

drugs used in this study were chosen such that they can be readily and safely achievable in human patients. Stem cells, in comparison with HepG2 cells, are resistant to drugs during the PIAF (Planning-, Information- and Analysis-System for Field Trials) (Cisplatin, Doxorubicin, 5-FU and Interferon) protocol, but when adding gold nanoparticle-coated drugs to the culture media, the results show a significantly lower survival rate of the tumor cells at 48 hours (Figure 3). Using Bonferroni's Multiple

Apoptosis flow cytometry analysis

Apoptosis-mediated cell death of LIV adult mesenchymal stem cells and CSC cells was examined by a double staining method using FITC-labeled Annexin V/PI apoptosis detection kit and analyzed by flowcytometry. The cells were analyzed after 24 hours exposure to a combination of drugs conjugated or unconjugated with GNP: doxorubicin + cisplatin + capecitabine + Pegylated interferon α-2b, correspondent to clinical chemotherapeutic protocol PIAF (***Table 2***). The apoptosis and death cell were high even in the control groups, possibly because of cell manipulation in course of trypsinisation and transport on ice.

Tab.8. *LIV and CSC cells assessed for apoptosis by flow-cytometry measurements show an increased percentage of dead and apoptotic cells for the samples treated with GNP-conjugated drugs (GNP-PIAF) in comparison with control group and cells treated with drugs alone.*

Sample	Early Apoptotic cells(%)	Late apoptotic +death cells (%)	Total apoptotic cells
LIV control	**1.63**	**21.31**	**22.94**
LIV treated with GNP-PIAF	**1**	**60.3**	**61.3**
LIV treated with PIAF	**3.7**	**41.2**	**44.9**
CSC control	**9.7**	**6.2**	**15.9**
CSC treated with GNP-PIAF	**8**	**27.9**	**35.9**
CSC treated with PIAF	**0**	**26.1**	**26.1**

The percentage of total apoptotic cells (early apoptotic cells positive only for V annexin + late apoptotic and death cells positive for both V Annexin and PI) show a greater apoptotic index for LIV cells, even in control samples, slow increase of proportion of apoptotic cells treated with drugs alone (1.1 folds in comparison with control gruop) and a greater increase of apoptotic cells treated with GNP-conjugated drugs (1.95 folds). CSC cells were more sensitive to chemotherapy: The percent of apoptotic and death cells increased 1.64 folds in comparison with control sample and with 2.25 folds for GNP-conjugated drugs (***Tab.8***).

I.4.4 Applications of functionalized gold nanoparticles-Temodal in glioblastoma multiform cancer

The cellular uptake efficiency is an important parameter and affects the therapeutic results. The visualization of GNPs-L-Aspartate-TMZ intake after 24h was monitored in contrast pase white light is presented in ***Fig.69a,b.*** A carefull look in contrast phase microscopy shows that *GNPs-Asp-TMZ* are internalized within the first hour . After 24 h and *the number of cells cells were affected and morphological changes occurredt suggesting a pre-apoptotic stage. Gold nanoparticles accumulation were visualized as black inclusions in perinuclear space.(**Fig.69a,b)***

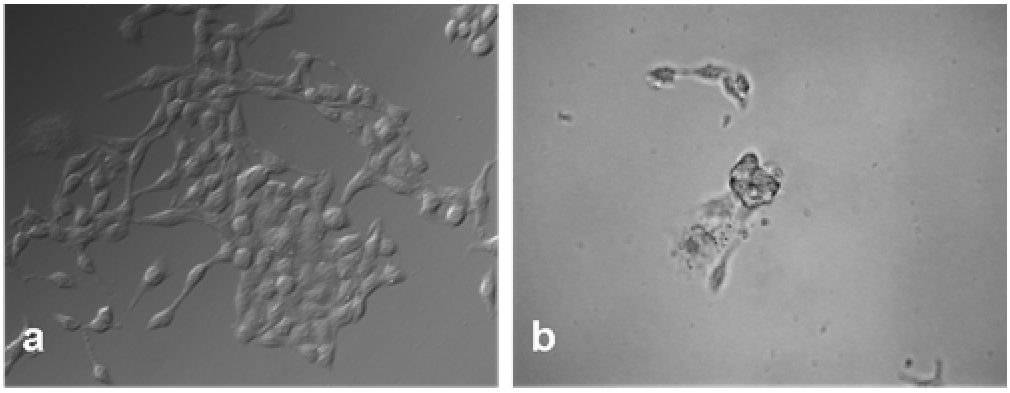

Fig.69a,b *GNPs-L-Aspartate-TMZ* incorporation after 24h (a) malignat glioma stem cells, control, (white light microscopy, PlasDIC contrast phase, magnification 400x),(b, c,d) intacke and internalisation of *GNPs-L-Aspartate-TMZ after 24h, (*PlasDIC phase contrast, magnification 400x)

MTT citotoxicity assay

A very common method of evaluating the effects of different substances in cell culture is MTT assay used to measure the mitochondria function of the cells in the culture dish. Glioma-derived stem cells were initially resistant to temozolomide , but when adding GNPs-Aspartate-TMZ to the culture media, the results show a reduced survival of the tumor cells. Cell proliferation assays clearly demonstrates the differences between conventional chemotherapy and TMZ-loaded GNPs. (***Fig.70***)

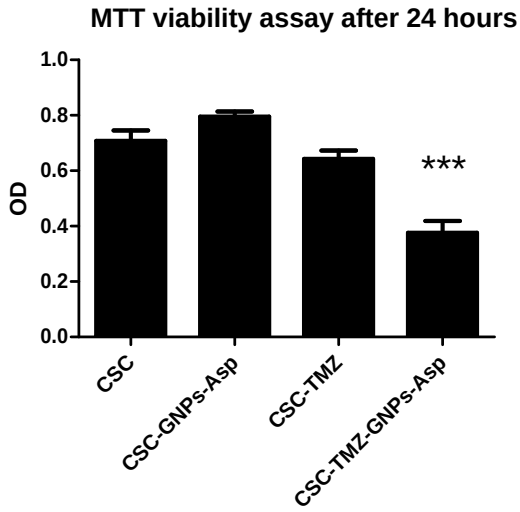

Fig.70. ***MTT viability assay results***

Using Bonferroni's Multiple Comparison Test, we found statistically significant results ($P<0.05$) between CSC vs. CSC -GNP s-TMZ (95% CI of 0.09214 to 0.5345. When one or more initiating genetic changes appeared at the progenitor level, all of the downstream cells continued this change. In one particular case, it is possible that a daughter cell acquired not only the properties of the stem cell, but also the additional alterations that allow the glioma to progress to the next step and invade surrounding tissues. The efficiency rate of the GNPs-Asp-TMZ system on glioblastoma-derived stem cell is approximately 50% higher compared with the alkali drug temozolomide.

V-Annexin/Pi apoptosis tests

Measuring Annexin V binding to the cell membrane, by conjugating FITC it is possible to identify and quantitate apoptotic cells on a single-cell basis by flow cytometry or fluorescence microscopy. Staining cells simultaneously with FITC-Annexin V (green

fluorescence) and the non-vital dye propidium iodide (red fluorescence) allows (bivariate analysis) the discrimination of intact cells (FITC-PI-), early apoptotic (FITC+PI-) and late apoptotic or necrotic cells (FITC+PI+). We performed the apoptotic tests by flowcytometry method and fluorescence microscopy. Analyzing the results in flowcytometric apoptosis assay we observed a slight increase of apoptosis in GNP-treated cells (apoptotic cells represents 10.7 % from total cells by comparison with the level in control cells-0.8%), aspect that was not found in microscopy apoptosis test (0.9% vs control cells 1.24%). This observation can be explained by the possibility of a mechanical stress affecting the cells loaded with nanoparticles during the centrifugation step in the flowcytometric method, a step that missed in the microscopy test. Both apoptosis tests revealed an increase of apoptosis of GNP-conjugated with TMZ. We notice a dramatic enhancement of late apoptosis in the case of flowcytometric test (78.3%), a value that represents a 1.9 fold increases within 24 hours compared with the apoptotic of cell treated with TMZ alone (31.1%). In the microscopic analysis were obtained similar results with the observation that apoptotic index of cells treated with TMZ-conjugate to GNP were 3.41 times higher than cells treated with TMZ. (***Tab 9***)

Table 9 Comparative presentation of double staining with V-Annexin/Pi apoptosis results obtained with flowcytometry (F) and microscopy(M) method***:*** *percentage of early, late and total apoptotic glioblastoma-derived CSCs*

Sample	**% Early Apoptotic cells**		**% Late apoptotic +Dead cells**		**Total**	
	F	**M**	**F**	**M**	**F**	**M**
CSC control	**0.4**	**1.24**	**0.4**	**0**	**0.8**	**1.24**
CSC control with GNP	**6.6**	**0.9**	**4.1**	**0**	**10.7**	**0.9**
CSC treated with TMZ	**10.8**	**7.05**	**31.1**	**0**	**41. 9**	**7.05**
CSC treated with TMZ-GNP	**4.4**	**24.07**	**78.3**	**0**	**82. 7**	**24.07**

Phase contrast and fluorescent microscopy of V-Anexin FITC/PI staining of adherent CSC treated with TMZ and GNP-conjugated TMZ, highlight important

morphological changes of cell number and shape and positivity for V-Annexin in the case of GNP-TMZ treated cells.(***Fig.71***)

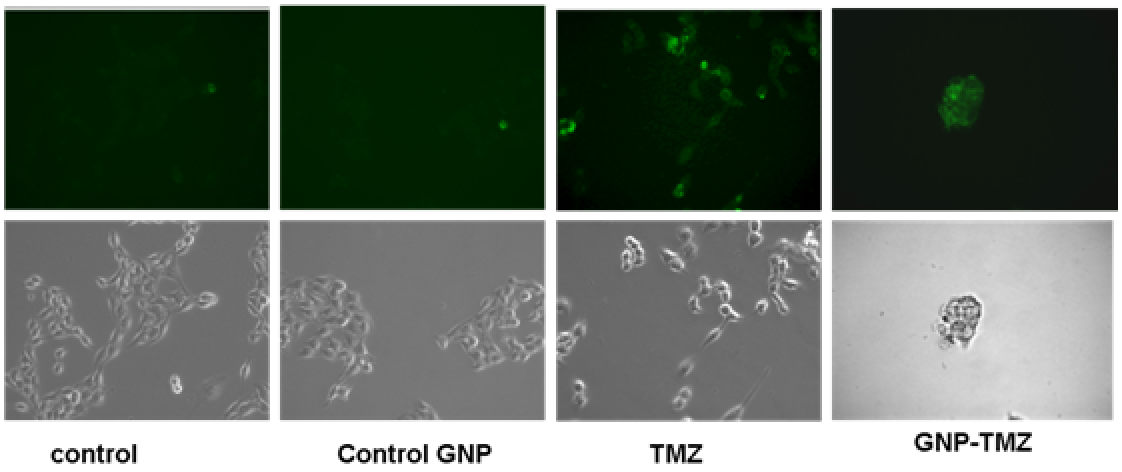

Fig. 71 *Morphologic aspects of apoptosis in V-Annexin FITC/PI staining observed in contrast phase and florescent microscopy (magnification x400). In upper panel is the correspondent image in fluorescence of images obtained in white light microscopy(lower pane)l.*

II. **Controlled destruction of subcellular structures in cancer therapy**

Introduction

Irradiation of HeLa cells containing gold nanoparticles in endosomes, cause endosomal rupture, migration of nanoparticles into the cytoplasm and finally cell death. This phenomenon of destruction of cancer cells can be controlled simultaneously by several factors: laser power, time of exposure to radiation, diameter of particles and their concentration. The mechanism behind this controlled death is achived by a photochemical mechanism. The laser radiation might induce radicals that destroies the cancer cells by migration of those radicals from endosoms into cytoplasm and causing cell death.

The purpose of the paper was to highlight how different laser power, exposure time and concentration of the particles can influence the mechanism of destruction and can control the cell death. The studies were performed on HeLa cells containing 15-16 nm gold nanoparticles (stabilized with citrate) which were irradiated with an continuous argon laser. The irradiation of the laser was set at 514 nm, value close to the plasmon absorption

band of citrate-gold nanoparticles (525 nm). The destruction of the cells was monitored by TEM and optical microscopy. Cell viability was tested with the viability test -trypan blue.

Experimental Details

Gold nanoparticles. Gold nanoparticles of 15-16 nm diameter with a narrow size distribution were prepared following the Turkevich-Frens procedure. Briefly, 50 μmol (19.7 mg) of HAuCl4 x 3H2O were dissolved in 150 ml of milli-Q water and heated to boiling. Subsequently, 1% w/w aqueous trisodium citrate solution, previously warmed to ca. 80°C was added (4.5 ml), and the mixture was refluxed for 30 minutes. The solution was then allowed to cool to room temperature under vigorous stirring overnight. The ruby red sol was characterised by UV-vis spectroscopy observing the typical plasmon band at 525 nm. The particle size was determined by TEM

Cell culture. HeLa cells were cultured in 3 cm culture dishes at 37°C in a humidified atmosphere of 5% CO2 in DMEM cell culture media containing 10% heat-inactivated fetal bovine serum, 1% penicillin-streptomycin and 1% non-essential amino acid solution. Passages 2-29 were used for the experiments; cells were typically grown to 60-80% confluency before splitting and re-seeding at 20-30% confluency the day before an uptake experiment. The uptake experiments were carried out at approximately 70% confluency.

Nanoparticle uptake and laser irradiation. HeLa cells were incubated with citrate coated gold nanoparticles dispersed in cell culture media for 1h, 3h, 9 h, 24 h at a final concentration of 2 nM. After incubation the excess of nanoparticles was removed and cells were rinsed twice with 2 ml of warmed PBS (1X) buffer. For laser irradiation, the cells were left in 2 ml PBS, and the irradiation area was marked precisely prior to laser illumination. The cultures were exposed to the 514 nm unfocused beam of a continuous-wave (cw) argon laser (Coherent Innova 300C), with a diameter of 1.55 mm. The cells were irradiated at several laser powers: 0.5 W, 1 W, 1.5 W for different times (30 sec, 1

min, 1:30 min, 2 min) with the laser beam directed onto the sample from above through the PBS.

Transmission Electron Microscopy (TEM). Immediately after irradiation, the cells were fixed by addition of 4% paraformaldehyde/2.5% glutaraldehyde in phosphate buffer (0.7 ml) for 1 h. Then the cells were rinsed with PBS buffer, post-fixed using 1% aqueous solution of OsO4 (0.5 ml) for 1 h. Subsequently the cells were washed with milli-Q H20, 30% ethanol solution and stained with 0.5% uranyl acetate (0.5 ml, in 30% ethanol) for 1 h. Cells were then gradually dehydrated using a series of ethanol solutions (30, 60, 70, 80 and 100%) and embedded in epoxy resin. The resin was polymerised at 60°C for 48 h. Ultrathin sections (70-100 nm) were cut using a diamond knife on a Leica Ultramicrotome and mounted on Formvar coated copper grids. The sections were then post-stained with 5% uranyl acetate in 50% ethanol and 2% aqueous lead citrate solution and imaged with FEI Tecnai Spirit TEM at 100 kV using AnalySIS software (Soft Imaging Systems).

AES analysis. HeLa cells cultured in 3 cm culture dishes were incubated with citrate particles for 1h, 3h, 9 h and 24 h as above. After the incubation the excess of nanoparticles was removed and cells were rinsed twice with 2 ml of warmed PBS (1X) buffer. Subsequently the cells were detached from the bottom of the dish (by using 0.2 ml trypsine) and redispersed in aqua regia to a finall volume of 15 ml.

Optical images were used to quantify the degree of cell death in different experimental conditions such as laser power, laser exposure time, concentration of gold nanoparticles. The results served to quantify the cell destruction and also to elucidate the mechanism that underlies this process.

Results and discussions

At high concentrations of nanoparticles, 24 h incubation time, and high intensity (1.5 W) approximately 90% of cells died (***Figure 1c***), the percentage of cell death (measured 23 minutes after irradiation, see below) is reduced from 51.73% to repectivelly

3.7% with decreasing laser intensity from 1W to 0.5 W (**Figure b, a**). By decreasing the incubation time to 9h, we observed that the procentage of cell death is almost similar with the procentage obtained for 24 h incubation.(20.67% dead cells for 0.5 W, 48.57% for 1W and 80.7% for 1.5 w)(***Figure 1. d,e,f***)

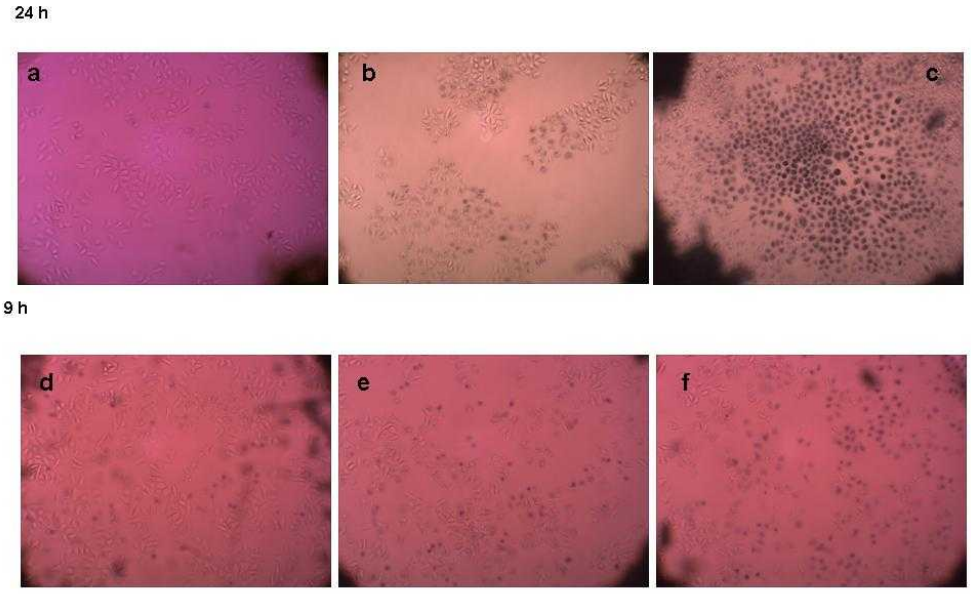

Figure 1: optical microscopy images of cells incubated with nanoparticles for 24 h (a, b, c) and 9 h (***d, e, f***) and laser power of 0.5 W (***a, d***), 1W (b, e) and 1.5 W (***c, f***) images were performed at 23 min after irradiation

Note that, around 9h incubation time the saturation is reached, therefore this incubation time was analysed in more detailed by using electron microscopy. TEM analysis were performed at 3 min and 23 min after irradiation with 0.5 W. (***Figure 2***)

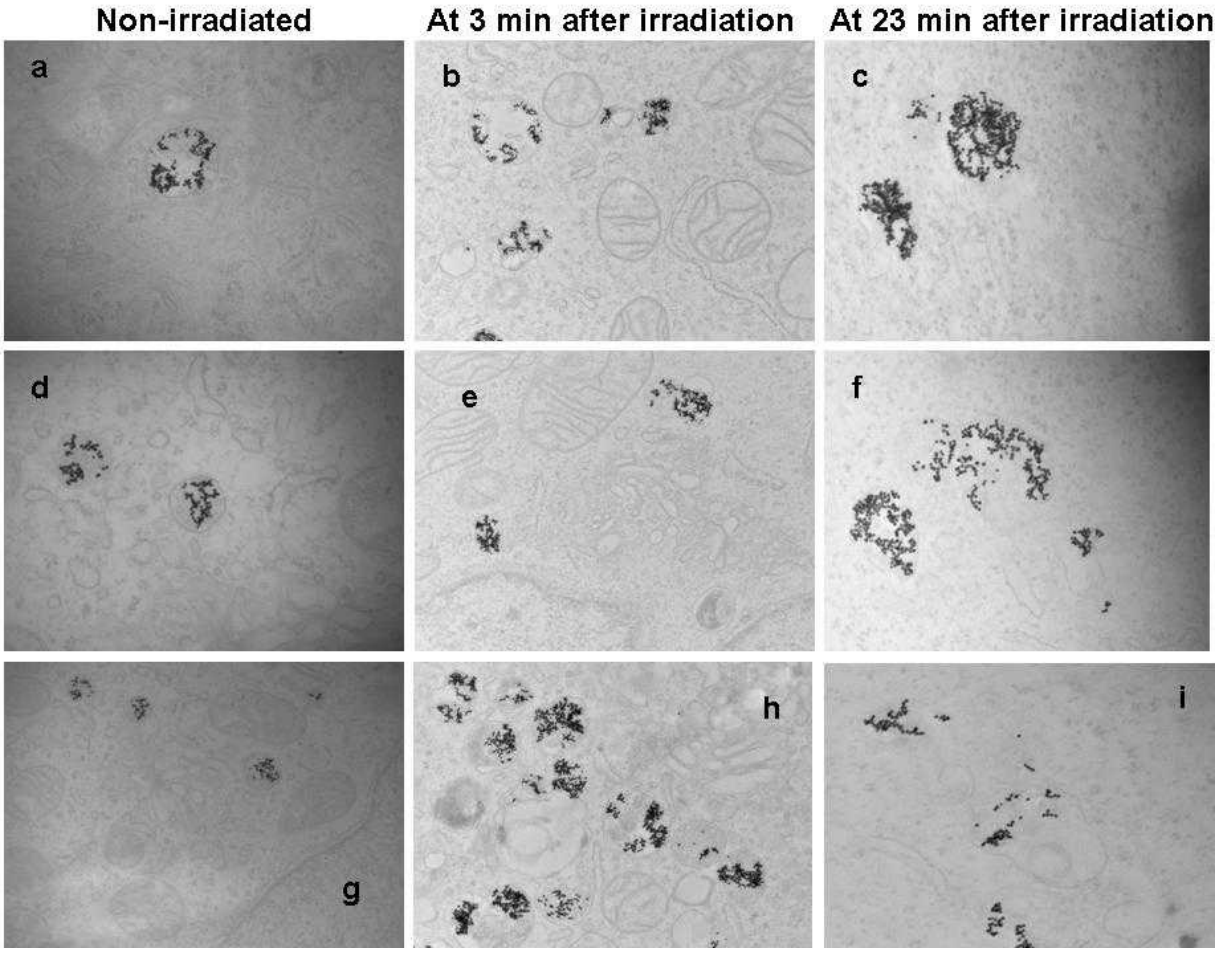

Figure.2 TEM images at 3 min ***(b,e,f)*** - 24 min ***(c,f,i)*** after irradiation compared with nonirradiated cells- ***(a,d,g)***

The TEM images of non-irradiated cells shows that particles are trapped inside the cell in endosomes, no endosomal escape occurred and no nanoparticles were found in the cytosol (***Figure2 a,d,g***) while at 3 minutes after radiation the endozomal membrane begins to destroy (***Figure2 b, e, f***) and after 23 min it disintegrate completely and the nanoparticules seem more dispersed throughout the cell, (***Figure 1 c,f, i***).

The concentration of gold nanoparticles is a significant parameter which influence the cells death, by decreasing the incubation time from 9h to 3h and respectively 1h the absorption coefficient decreases, and the percentage of cell death is reduced. The ***figures 3 a,b,c*** presents the results for 3h incubation, respectively 1h (figure 3 d,e,f) at different laser powers of 0.5 W (***a, d***), 1 W (***b, e***) and 1.5 W (***c, f***). By quantifing the cells death the

results are: from 15.21% (1h)-to 13, 96% (3h) for 0.5 W,

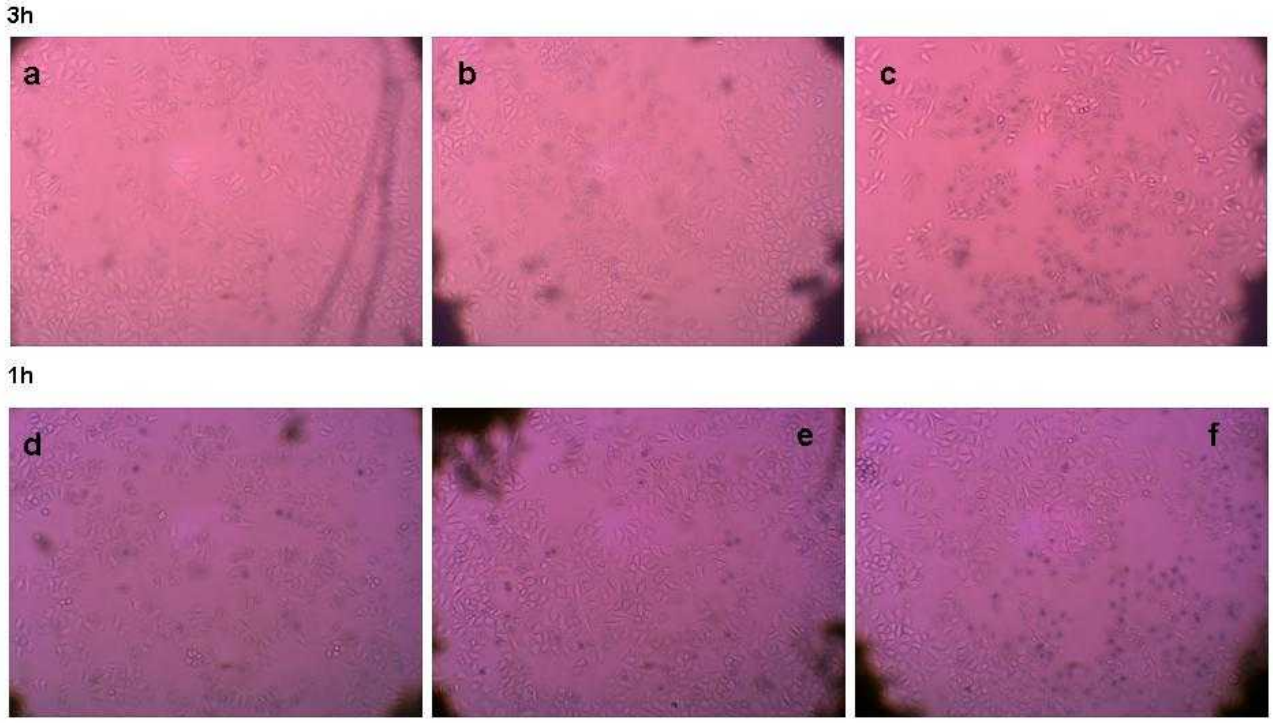

Figure 3: optical microscopy images of cells incubated with nanoparticles for 3 h (***a, b, c***) and 1 h (***d, e, f***) and laser power of 0.5 W (***a, d***), 1W (b, e) and 1.5 W (***c, f***). The images were made at 23 min after irradiation

Another critical parameter that influence the cell death is *laser exposure time*. By increasing the exposure time the mortality increases. Tipical images for different irradiation times using a laser power of 1, 5 W and the concentration of particles coresponding to 9 h of incubation are presented in ***Figure 4***

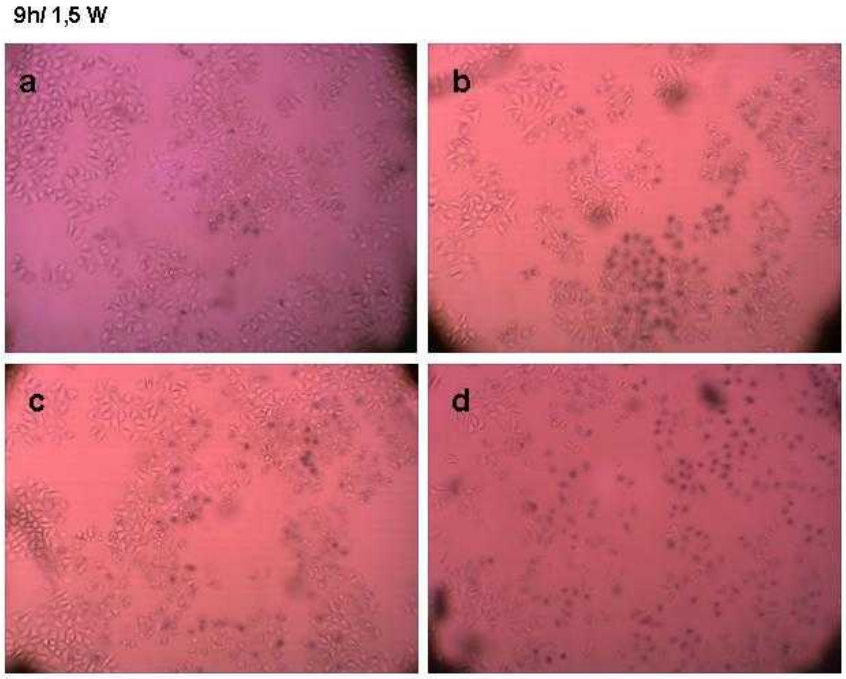

Figure 4*: Optical microscopy images of cells irradiated for 30 sec (**a**) and 60 sec (**b**) 90sec (**c**), 120 sec (**d**) with 0.5W The images were made at 23 min after irradiation The incubation time is 9 h.*

II.1.1**Influence of gold nanoparticle concentration and laser power**

The laser power and concentration of nanoparticles has a major influence on the cell destruction and death. To highlight how this factors influence the degree of destruction we worked at three laser powers: 0.5 W, 1 W and 1, 5 W and four concentration 1h, 3h, 9h, 24h incubation. The irradiation time was constant in all cases, 2 minutes.
The results are shown in ***Figure 5 a, b, c.***

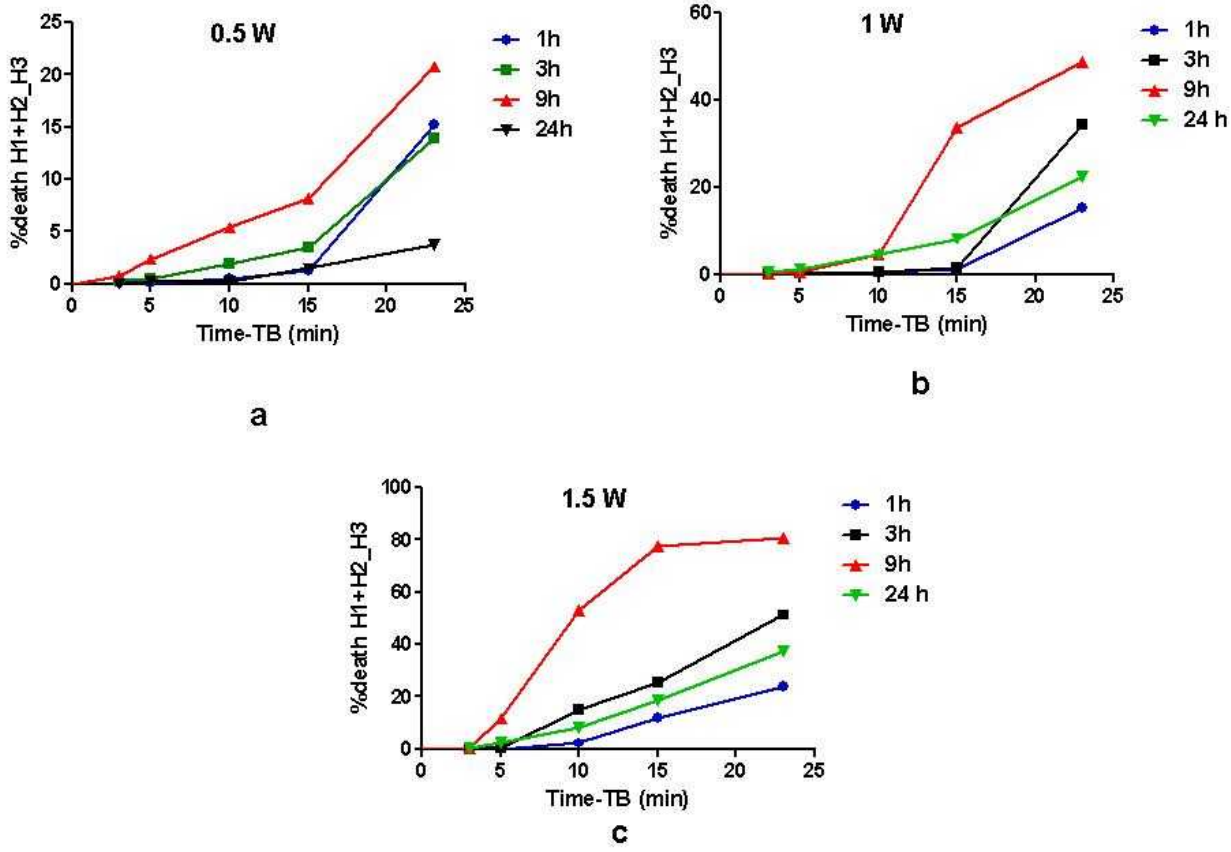

***Figura 5 a, b, c** : Time destruction of cancer cells influenced by laser power and nanoparticles concentration: for 0, 5 w –incubation time 1, 3,9,24 h (**a**), 1 w –incubation time 1, 3,9,24 h (**b**), 1,5 w- incubation time 1, 3,9,24 h (**c**)*

In all cases the points in the diagrams represents the average of three parallel measurements.

Figure 5 shows that at low concentrations of gold (1h) using any of the laser power (0,5 W or 1 W or 1,5 W) the procentage of death is very low and it does not exceed 20% (the value for 1.5 W). By increasing the laser power the cell begin to dye more early: for 0.5 W they begin to dye at 5 min after irradiation while for 1.5 W the induction time is at 10 min.

By increasing incubation time and power of the laser the procentage of cell death increase

but only at high laser power 1 W and respectively 1,5 W. We note that at a low power 0.5 W, the degree of damage decreases at from 15% (incubation time 1 h) to13.96% (3h incubation time) and from 20% (9 h incubation) to 3.74% (24 h incubation). This abnormality can be attributed to the measurement errors, wich usually appears because of cells defense abilities.

For 1 w and 1,5 w the mortality increases by increasing the incubation time. A big jump on the degree of destruction is found for 9 and 24 h incubation time compared with the incubation time 1 and 3 h. The values for 9 h and 24 h incubation are very close: 1W- 48,61% (9h incubation time)/51.73% (24 h incubation time), 1.5 W- 80.82 (9h incubation time)/88.01% (24 h incubation time).

At the irradiation power 1W the curves have almost the same slope, showing that the destruction of the cells is made by the same mechanism. At 1.5 W the curves practically overlap after 10 minutes. Also, the slope of the curves shows that the chemical reaction between free radicals and the cell membrane takes place very quickly.

Figure 6 shows the influence of concentration (1h, 3h, 9h, 24 h- incubation time) at three laser powers:0.5 W, 1 W and 1.5 W.

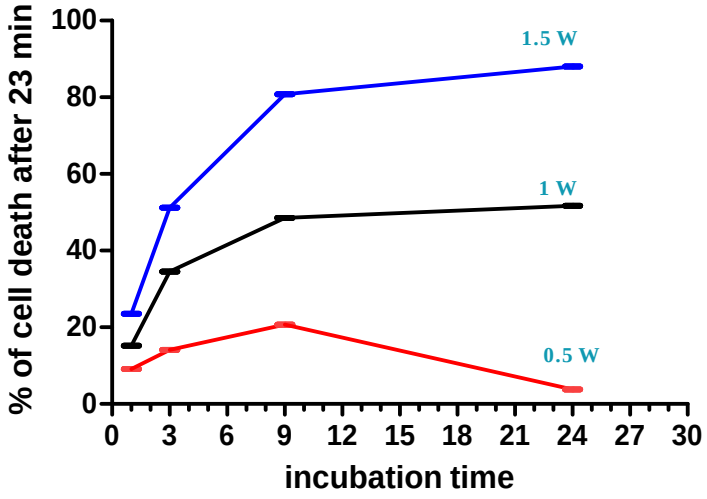

Figure 6*: Influence of concentration (1h, 3h, 9h, 24 h- incubation time) at three laser powers: 0.5 W, 1 W and 1.5 W*

II.1.2 **Influence of laser exposure time**

We've seen in the previous section that the laser intensity plays a decisive role in the dynamics of cancer cell death. Increasing the power of irradiation the of electrons energy from the Fermi level increases. In these conditions a large number of electrons will form free radicals. The energy of the electrons is also dependent on the laser exposure time. ***Figure 7*** shows the distruction of the cells at different exposure time. The results are the average of three measurements made in parallel.

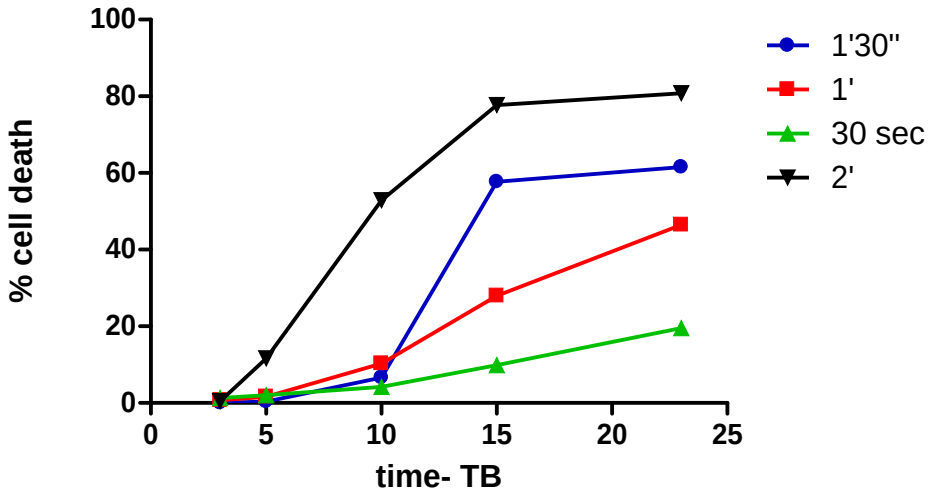

Figure 7: Influence of irradiation time: 2 min, 1.5 min, 1 min, 30 sec on the cell death, when cells were irradiated with 1.5 W and the particles incubation time was 9h. cell death measured after 23 minutes

After the first three minutes the cells are still alive, the endosomal membrane is starting to disolve (this is confirmed also by the TEM pictures), the cells are stressed and begin to fight due to its self-defense system. However, at a high exposure (2 min) few cells are death after 3 min while an abundent ammount of cell are starting to die after 5 min. The number of cell death increase liniar from 5 min to 15 min, and at 23 min almost all the cell are death. Decreasing the exposure time to (1 min, 30 sec) the dying starts at 10 min.

In this case the death is increasing liniar while for higher exposure times, 1.5 min is exponential. This suggests that the mechanism of dying is a complex one; it involves the radicals formation and their diffusion into cytosol and finally cell death.

Considering that the destruction of cancer cells (the reaction between free radicals with the cell membrane) , occurs after a first order reaction by representing -ln (1-ή) = kt (where ή is the degree of mortality-and t- the reading time after irradiation, k-rate constant process of cell death), we obtain the representations from **Figure.8**. (The curves slopes are the rate constant, k)

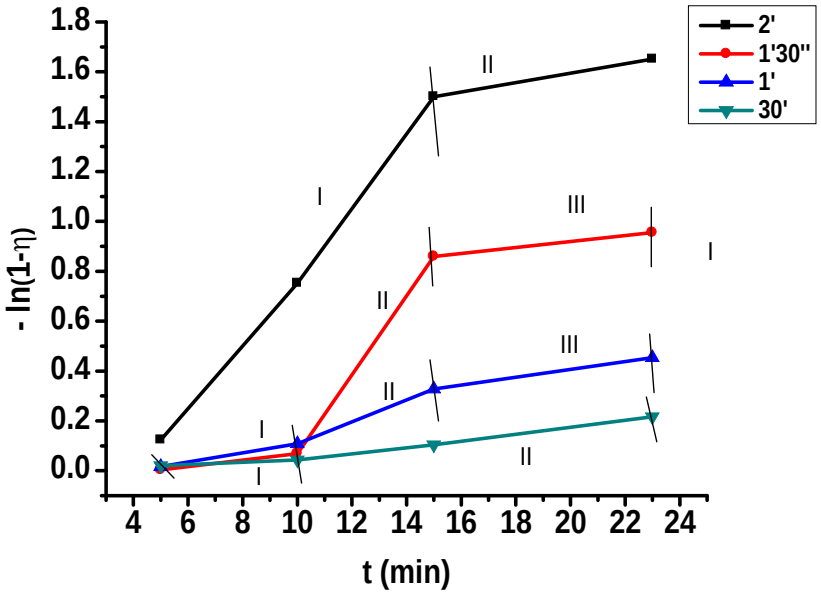

Fig.77: Plot of- ln (1-ή) - t

The rate constant values were calculated from the curve slopes and are given above in

Tab.9

The rate constant values for 9 h incubation time sample

t	30 sec	1 min	1 min 30 sec	2 min

K x 10-4	**I**	**Î I**	**I**	**II**	**III**	**I**	**II**	**III**	**I**	**Î I**
Min -1	**0,73**	**2.26**	**2.35**	**5,42**	**2.8**	**2.07**	**27.7**	**2,1**	**24**	**3.3**

The representations -ln (1-ή) - t leads to lines with different slopes, which shows that practically the destruction of cancer cells occur by a mechanism that involve one two or even three steps.

The plot for **2 min and respectively 30 sec** irradiation time has two domains with two different constant values. From here we presume that for this irradiatin time a two-step mechanism is involved in the cell distruction.

The rate constant for 2 min irradiation has the values: 24 x10-4 for the I-st domain and 3.3 x10-4 for the second. Comparing this two values with the values obtained for 30 sec irradiation time (0.73-2.26 x10-4) it is found that rate constant for 2 min, is with two orders bigger in the I- st domain and has the same value in the II- nd domain. The big difference in the I-st domain for 3 min irradiation can be attributed to the large number of free radicals that are formed at high irradiation times, radicals that provides high reaction rate (a rapid destruction of the endosomal membrene) and a slow diffusion into cytosol. The same order values from domanin II can be explained by the small number of free radicals that exist in the both cases, radicals wich give a low rate of destruction.

For the irradiation time 1 min 30 sec and 1 min, there are three domains. Between [10-15 min] (domain II) in both curves have the same slope. The destruction occurs very fast and is made by the same mechanism. Outside this range (in the domain I and III) cell destruction process is carried out by similar mechanisms with that from irradiation time 30sec and 2 min.

The process of cancer cells destruction is very complex and is influenced both by the concentration of free radicals at the thought that they depend on the irradiation time, laser power, concentration of nanoparticles (in this case determined by incubation time)

Bibliografie

1) Ebbesen T, Ajayan P. Large-scale synthesis of carbon nanotubes. Nature 1992;358(6383):220-222.

2) Iijima S, Ichihashi T. Single-shell carbon nanotubes of 1-nm diameter. Nature 1993;363(16): 603 – 605

3) Bethune D, Klang C, De Vries M, Gorman G, Savoy R, Vazquez J, et al. Cobalt-catalysed growth of carbon nanotubes with single-atomic-layer walls. *Nature* 1993;363(16): 605 – 607.

4) Kratchmer W, Lamb L, Fostiropoulos K, Huffman D. Solid C60: a new form of carbon. Nature 1990;347(12):354-358.

5) Seraphin S. Single-walled tubes and encapsulation of nanocrystals into carbon clusters, J. Electrochem.Soc. 1995;142(10):290–297.

6) Thess A, Lee R, Nikolaev P, Dai H, Petit P, Robert J, et al. Crystalline ropes of metallic carbon nanotubes. Science 1996;273(5274):474-483.

7) Journet C, Maser W, Bernier P, Loiseau A, Lamy de La Chapelle, M., Lefrant S, et al. Large-scale production of single-walled carbon nanotubes by the electric-arc technique. Nature 1997;388(6644):756-757.

8) Kong J, Cassell AM, Dai H. Chemical vapor deposition of methane for single-walled carbon nanotubes. Chem Phys Lett 1998;292(4-6):567-574.

9) Cassell AM, Raymakers JA, Kong J, Dai H. Large scale CVD synthesis of single-walled carbon nanotubes. J Phys Chem B 1999;103(31):6484-6492.

10) Pan L, Shoji T, Nagataki A, Nakayama Y. Field emission properties of titanium carbide coated carbon nanotube arrays. Adv Mat 2007;9(7):584-587.

11) Xiao R, Cho SI, Liu R, Lee SB. Controlled electrochemical synthesis of conductive polymer nanotube structures. J Am Chem Soc 2007;129(14):4483-4489.

12) Yan Y, Zheng W, Su L, Mao L. Carbon Nanotube Based Glucose/O2 Biofuel Cells. Adv Mater 2006;18(19):2639-2643.

13) S. A. Hooker, R. Geiss, R. Schilt, A. Rand Kar, ''Elevated temperature QCM for nanotube quality control'', Amer. Cer. Soc, 1997;58(1):43-58,

14) Suh DJ, Kwak C, Kim JH, Kwon SM, Park TJ. Removal of carbon monoxide from hydrogen-rich fuels by selective low-temperature oxidation over base metal added platinum catalysts. J Power Sources 2005;142(1-2):70-74.

15) Li H, Rosario A, Davis S, Glass T, Holland T, Davis R, et al. Network formation of vinylester-styrene composite matrix resins. J Adv Mater 1997;28(4):55-62.

16) Klabunde KJ, Richards R. Nanoscale materials in chemistry. Poly and Mater, 2002;11(2):121-167.

17) Artemov D, Mori N, Okollie B, Bhujwalla ZM. MR molecular imaging of the Her-2/neu receptor in breast cancer cells using targeted iron oxide nanoparticles. Mag Res Med 2003;49(3):403-408.

18) Forbes ZG, Yellen BB, Barbee KA, Friedman G. An approach to targeted drug delivery based on uniform magnetic fields. Magnetics, IEEE Transactions 2003;39(5):3372-3377.

19) Cao YC, Jin R, Nam JM, Thaxton CS, Mirkin CA. Raman dye-labeled nanoparticle probes for proteins. J Am Chem Soc 2003;125(48):14676-14677.

20) Molday RS, Mackenzie D. Immunospecific ferromagnetic iron-dextran reagents for the labeling and magnetic separation of cells. J Immunol Methods 1982;52(3):353-367.

190) Thomas KG, Zajicek J, Kamat PV. Surface binding properties of tetraoctylammonium bromide-capped gold nanoparticles. Langmuir 2002;18(9):3722-3727.

191) Selvakannan P, Mandal S, Phadtare S, Pasricha R, Sastry M. Capping of gold nanoparticles by the amino acid lysine renders them water-dispersible. Langmuir 2003;19(8):3545-3549.

192) Ongaro A, Griffin F, Beecher P, Nagle L, Iacopino D, Quinn A, et al. DNA-templated assembly of conducting gold nanowires between gold electrodes on a silicon oxide substrate. Chemistry of materials 2005;17(8):1959-1964.

193) Graham JS, Miron Y, Grandbois M. Assembly of collagen fibril meshes using gold nanoparticles functionalized with tris(hydroxymethyl)phosphine-alanine as multivalent cross-linking agents. J Mol Recognit. 2011;24(3):477-82

194) Zhong Z, Patskovskyy S, Bouvrette P, Luong JHT, Gedanken A. The surface

chemistry of Au colloids and their interactions with functional amino acids. The Journal of Physical Chemistry B 2004;108(13):4046-4052.

195) Zhong Z, Luo J, Ang TP, Highfield J, Lin J, Gedanken A. Controlled organization of Au colloids into linear assemblies. The Journal of Physical Chemistry B 2004;108(47):18119-18123.

196) Shao Y, Jin Y, Dong S. Synthesis of gold nanoplates by aspartate reduction of gold chloride. Chem.Commun. 2004(9):1104-1105.

197) Zhong Z, Subramanian AS, Highfield J, Carpenter K, Gedanken A. From discrete particles to spherical aggregates: a simple approach to the self-assembly of Au colloids Chemistry 2005;11(5):1473-1478.

198) Polavarapu L, Xu QH. A single-step synthesis of gold nanochains using an amino acid as a capping agent and characterization of their optical properties. Nanotechnology 2008;19(2):075601.

201) Barnes WL, Dereux A, Ebbesen TW. Surface plasmon subwavelength optics. Nature 2003;424(6950):824-830.

202) Tang Z, Kotov NA. One-Dimensional Assemblies of Nanoparticles: Preparation, Properties, and Promise. Adv Mater 2005;17(8):951-962.

203) Cohen-Karni T, Timko BP, Weiss LE, Lieber CM. Flexible electrical recording from cells using nanowire transistor arrays. Process Nat Acad of Sci 2009;106(18):7309.

204) Kiely C, Fink J, Zheng J, Brust M, Bethell D, Schiffrin D. Ordered colloidal nanoalloys. Adv Mater 2000;12(9):640-643.

205)Lin S, Li M, Dujardin E, Girard C, Mann S. One-Dimensional Plasmon Coupling by Facile Self-Assembly of Gold Nanoparticles into Branched Chain Networks. Adv Mater 2005;17(21):2553-2559.

208) Castaneda L, Valle J, Yang N, Pluskat S, Slowinska K. Collagen cross-linking with Au nanoparticles. Biomacromolecules 2008;9(12):3383-3388.

209) Mahl D, Greulich C, Meyer-Zaika W, Köller M, Epple M. Gold nanoparticles: dispersibility in biological media and cell-biological effect. J.Mater.Chem. 2010;20(29):6176-6181.

210) Harris JR, Reiber A. Influence of saline and pH on collagen type I fibrillogenesis in vitro: fibril polymorphism and colloidal gold labelling. Micron 2007;38(5):513-521.

211) Orza A, Soritau O, Olenic L, Diudea M, Florea A, Rus Ciuca D, et al. Electrically Conductive Gold-Coated Collagen Nanofibers for Placental-Derived Mesenchymal Stem Cells Enhanced Differentiation and Proliferation. ACS Nano 2011;5(6):4490-503

229) Yang XR, Xu Y, Yu B, Zhou J, Qiu SJ, Shi GM, et al. High expression levels of putative hepatic stem/progenitor cell biomarkers related to tumour angiogenesis and poor prognosis of hepatocellular carcinoma. Gut 2010;59(7):953.

230)Parkin DM, Bray F, Ferlay J, Pisani P. Estimating the world cancer burden: Globocan 2000. International Journal of Cancer 2001;94(2):153-156.

235) Kim BY, Rutka JT, Chan WC. Nanomedicine. N Engl J Med. 2010;363(25):2434-2443

CURRICULUM VITAE

Name: Anamaria Ioana Orza
Office Address: Department of Organic Chemistry, Nanoscience
E-mail: anamariaorza@gmail.com
Home Address: 21 Decembrie 1989 Street, no.5, Cluj-Napoca
Date of Birth: September 30, 1986
Place of Birth: Sighetu-Marmatiei
Nationality: Romanian
Marital Status: Not Married

EDUCATION:

2008-present:

PhD student (Nanotechnology) **Babes- Bolyai University, Faculty of Chemistry and Engineering Chemistry**

Research Project:

Synthesis and Physical-Chemical characterisation of some metallic nanostructurated compounds. Aplications in electronics and medicine

Research experience:

- Preparation of various nanostructures base nanoparticles, UV-VIS, FTIR, TEM, NMR, I-V characterisation of these nanostructures.
- Cell culture assay

Conference

- National

'' Natural and Synthesized products applied in medicine '', 25 november 2009, Cluj Napoca, Romania

Poster Presentation: ''Collagen supported metallic nanowires'' , Anamaria Orza, Stela Pruneanu, Liliana Olenic, Adrian Florea, Mircea Diudea

Poster Presentation: ''Biomolecules with applications in molecular electronics'', Stela Pruneanu, Liliana Olenic, Anamaria Orza, A.Houtlon, B.R.Horracks

- **International**

RomPhyschem14, 2-4 july 2010, Bucharest, Romania
Poster Presentation,'Single-step synthesis of gold nanowires using biomolecules as capping agent/template. Applications for tissue engineering'**,** A. Orza[a*], C. Tomuleasa[b,c], O. Soritau[b], A. Florea[c], S. Pruneanu[d], L. Olenic[d], M. Diudea

7th International Conference on Applied Mathematics (ICAM7) in Nano-ERA", 1-4 septembrie 2010, Cluj-Napoca Romania

Oral Presentation,'' Highly Efficient Gold Nanoparticles Drug Delivery for in Vivo Therapy of malignant gliomas''Anamaria Orza, Olga Soritau, Ciprian Tomuleasca

- Workshosp:

III European Workshop in Drug Synthesis, 23rd to 27th May, 2010 Siena, Italy

Poster and Oral Presentation, ''Synthesis Characterization and Synergetic Effect of Gold Nanoparticle-Cisplatin/ Doxorubicin/ Capecitabine Vectors on Hepatic Cancer Stem Cells ,Anamaria Orza[1], Ciprian Tomuleasca[2,3], Olga Soriţ ãu[2], Olenic Liliana[4], Stela Pruneanu[4], Mircea Diudea[1]

Papers:

1. **Morphological and electrical characteristics of amino acid–AuNP nanostructured two-dimensional ensembles,** Anamaria Orza, Olenic Liliana, Stela Pruneanu, Florina Pogacean, Alexandru Biris**, Chemical Physics, Volume 373, Issue 3, 3 August 2010, Pages 295-299**

2. **Conductive Collagen-based Gold Nanoparticles for Placental-derived Mesenchymal Stem Cells Differentiation,** Anamaria Orza, Olga Soritau, Liliana Olenic, Mircea Diudea, Adrian Florea, Dan Rus Ciuca,Carmen Mihu, Daniel Casciano, Alexandru S. Biris, **ASC Nano, 2011;5(6):4490-503**

3. **Enhanced LASER thermal ablation for in vitro liver cancer destruction by specific delivery of multi wall carbon nanotubes functionalized with human serum albumin,** Cornel Iancu ,Constantin Bele, Cornel Catoi, Anamaria Orza, Flaviu A. Tabaran Rares Stiufiuc, Ariana Stir, Cristian Matea, Dana Iancu[1], Florin Zaharie, Teodora Mocan, Lucian Mocan, **International Journal of Nanomedicine**, 2011 6: 129–141

4. **Selective ex-vivo photothermal ablation of human pancreatic cancer with albumin functionalized multiwalled carbon nanotubes,** Lucian Mocan, Flaviu A Tabaran,Teodora Mocan, Constantin Bele, Anamaria Ioana Orza, Ciprian Lucan, Rares Stiufiuc, Ioana Manaila, Ferencz Iulia, Iancu Dana, Florin Zaharie, Gelu Osian, Liviu Vlad, Cornel Iancu, **International Journal of Nanomedicine 2011:6 915–928**

5. **Effect of gold nanoparticles conjugated with various anti-cancer drugs on lowering the chemoresistence of hepatic cancer stem-like** cells, Anamaria Orza[1,] Ciprian Tomuleasa[2], Olga Soritau[2], Olenic Liliana[3], Ioan Bratu[3], Mircea Diudea,[1] Sergiu Susman[2], Emoke Pall[5], Daniel Casciano[6], Alexandru S. Biris[6] ***-in pending ACS Nano***

6. **Temozolomide-loaded gold nanoparticles as an alternative chemotherapy option for inoperable recurrent malignant gliomas-** Anamaria Orza , Ciprian Tomuleasa, Liliana Olenic, Olga Soriţ ău, Adrian Florea, Ovidiu Pana,Ioan Bratu, Mircea Diudea, Alexandru S. Biris***, in pending ACS Nano***
7.

Patents:

1. **Synthesis and purification process for racemic acspartic acid used in biomedical and tehnical pruposes,** Anamaria Orza, Mitre Viorel, Mitre Ioana-**OSIM Pat.No.A/01075**
2. **Process for obtaining ultra short functionalized MWCNTs by controlled oxidation,** Matea Cristian Tudor, Bele Constantin, Iancu Cornel, Mocan Lucian, Orza Anamaria-Ioana-**OSIM Pat.No.A/ 01134**

2004 – 2008

- **Babes- Bolyai University, Faculty of Chemistry and Engineering Chemistry,** BSc (Chemistry) Degree - Result: A

Final Year Research Project:

Title: Synthesis, functionalization and characterization of some terpyridines metal complexes
Analyses results: H1-NMR, C13-NMR, MASS Spectroscopy

- University Babes- Bolyai, Faculty of European Studies, **Management Studies**

2000-2004

King Ferdinand High School Leaving Certificate**: 'A' grades in higher level Mathematics and Chemistry.**